MPPT CONTROL OF FULL-BRIDGE MICROINVERTER FOR STANDALONE PHOTOVOLTAIC APPLICATION

FATIN NURSYUHADA BINTI SHAHRIZAM

BACHELOR OF ELECTRICAL ENGINEERING WITH HONOURS
UNIVERSITI TEKNIKAL MALAYSIA MELAKA

2024

MPPT CONTROL OF FULL-BRIDGE MICROINVERTER FOR STANDALONE PHOTOVOLTAIC APPLICATION

FATIN NURSYUHADA BINTI SHAHRIZAM

A report submitted
in partial fulfilment of the requirements for the degree of
Bachelor of Electrical Engineering with Honours

Faculty of Electrical Technology and Engineering

UNIVERSITI TEKNIKAL MALAYSIA MELAKA

2024

DECLARATION

I declare that this thesis entitled "MPPT CONTROL OF FULL-BRIDGE MICROINVERTER FOR STANDALONE PHOTOVOLTAIC APPLICATION is the result of my own research except as cited in the references. The thesis has not been accepted for any degree and is not concurrently submitted in the candidature of any other degree.

Signature :

Name : FATIN NURSYUHADA BINTI SHAHRIZAM

Date : 28/06/2024

APPROVAL

I hereby declare that I have checked this report entitled "MPPT CONTROL OF FULL-BRIDGE MICROINVERTER FOR STANDALONE PHOTOVOLTAIC APPLICATION", and in my opinion, this thesis fulfils the partial requirement to be awarded the degree of Bachelor of Electrical Engineering with Honours.

Signature : ....

Supervisor Name : DR. WAHIDAH BINTI ABD HALIM

Date : 28/06/2024

DEDICATIONS

To my beloved mother and father

Monirah Binti Abdul Hamid@Noordin and Shahrizam Bin Md Haris@Md Ariff

My inspiring lecturers and friends.

ACKNOWLEDGEMENTS

In the name of Allah, the Most Gracious, the Most Merciful. I begin by expressing my heartfelt gratitude to Allah, the Almighty, the Lord of the universe, and I extend my praises and blessings upon Muhammad, His servant and messenger. Alhamdulillah, all praise be to God for His guidance and support, which has been instrumental in guiding me through the challenges of my Final Year Project I during this academic year.

I wish to take this opportunity to convey my deep appreciation to Dr. Wahidah Binti Abd Halim. Her invaluable guidance and unwavering support have played a crucial role in the successful completion of my project. I am grateful for her expertise and mentorship, which have significantly contributed to my academic journey. Furthermore, I extend sincere thanks to my esteemed panelists, Dr. Siti Azura Binti Ahmad and Associate Professor Dr. Raja Nor Firdaus Kashfi Bin Raja Othman, for their insightful feedback and constructive comments. Their guidance has not only enriched my project but will undoubtedly contribute to my continuous improvement as a student.

I would like to acknowledge the Faculty of Electrical and Technology Engineering (FTKE) at Universiti Teknikal Malaysia, Melaka for granting me the opportunity to pursue this project. The support and excellent facilities, including a well-equipped lab, provided by the faculty have greatly facilitated my work and learning experience. Finally, I extend my thanks to all individuals, both directly and indirectly involved in the completion of this assignment. May they find ease in all their endeavors and enjoy a prosperous life. Together, with gratitude and humility, I reflect on the collective effort and support that has shaped the successful culmination of this academic undertaking.

ABSTRACT

A solar panel is able to generate optimal power when it is constantly exposed to the maximum amount of solar radiation, which causes its output voltage and current to constantly reach their peak values. Determining whether the microinverter panel can reach maximum output power when connected to a solar panel is the goal of this research project. This is accomplished through the perpetual maintenance of the solar array at its Maximum Power Point (MPP). The project's objective is to develop and implement a comprehensive microinverter system, comprising a full-bridge DC-DC converter and a single-phase H-bridge inverter. The primary goals include achieving efficient power conversion and implementing maximum power point tracking (MPPT) control for optimal energy harvesting in photovoltaic applications. The project scope involves designing and analyzing the full-bridge DC-DC converter using MATLAB/Simulink, serving as the initial stage of the microinverter. Following this, a 500W power-rated DC-AC converter is integrated as the second stage, utilizing an H-bridge inverter. The project scrutinizes the efficiency of the MPPT controller for the full-bridge DC-DC converter to enhance the overall system performance. Additionally, a comparative analysis evaluates the microinverter's efficiency against a string inverter, providing insights into its operational effectiveness. The utilization of the H-bridge inverter for the DC-AC conversion stage enhances the versatility and robustness of the microinverter system. Ultimately, this project contributes to advancing the field of renewable energy systems by offering a detailed exploration of the microinverter's functionality and performance under various conditions.

ABSTRAK

Sebuah panel solar mampu menghasilkan kuasa optimum apabila terdedah secara berterusan kepada jumlah radiasi solar maksimum, yang menyebabkan voltan dan arus keluarannya sentiasa mencapai nilai puncak mereka. Menentukan sama ada panel penyongsang-mikro dapat mencapai kuasa keluaran maksimum apabila disambungkan kepada panel solar adalah matlamat projek penyelidikan ini. Ini dicapai melalui penyelenggaraan berterusan rangkaian solar pada Titik Kuasa Maksimumnya (MPP). Objektif projek ini adalah untuk membangunkan dan melaksanakan sistem mikroinverter yang komprehensif, yang terdiri daripada penukar AT-AT jambatan penuh dan jejambat-H satu fasa. Matlamat utama termasuk mencapai penukaran kuasa yang cekap dan melaksanakan kawalan titik kuasa maksimum (MPPT) untuk penuaian tenaga optimum dalam aplikasi fotovoltaik. Skop projek melibatkan reka bentuk dan analisis penukar AT-AT jambatan penuh menggunakan MATLAB/Simulink, berfungsi sebagai peringkat awal penyongsang-mikro. Selepas ini, sebuah penukar AT-AU berkuasa 500W diintegrasikan sebagai peringkat kedua, menggunakan penterjemah H-jambatan. Projek ini mengkaji kecekapan pengawal MPPT bagi penukar AT-AT jejambat penuh untuk meningkatkan prestasi keseluruhan sistem. Selain itu, analisis perbandingan menilai kecekapan penyongsang-mikro berbanding penterjemah tali, memberikan pandangan keberkesanan operasinya. Penggunaan jejambat-H untuk peringkat penukaran AT-AU meningkatkan kepelbagaian dan kekuatan sistem penyongsang-mikro. Pada keseluruhan, projek ini menyumbang kepada kemajuan dalam bidang sistem tenaga boleh diperbaharui dengan menawarkan penerokaan terperinci mengenai fungsi dan prestasi penyongsang-mikro dalam pelbagai keadaan.

TABLE OF CONTENTS

LIST OF TABLES

LIST OF FIGURES

LIST OF SYMBOLS AND ABBREVIATIONS

DC	-	Direct Current
MPPT	-	Maximum Power Point Tracking
AC	-	Alternating Current
PV	-	Photovoltaic
P-V	-	Power-Voltage
I-V	-	Current-Voltage
P&O	-	Perturb and Observe
IC	-	Icremental Conductance
V_{IN}	-	Input voltage
V_O	-	Ouput voltage
G	-	Voltage Gain
$D_{1,2,3}$	-	$Diode_{1,2,3}$
D	-	Duty cycle
T	-	Transformer
L	-	Inductance
C	-	Capacitor
R	-	Resistor
$S_{1,2,3,4}$	-	MOSFET
n	-	Turns ratio

LIST OF APPENDICES

CHAPTER 1

INTRODUCTION

1.1 Project Background

The world's energy consumption has been rising due to both technical developments and global growth. It has led to much higher energy expenditures, and greater energy demand has increased greenhouse gas emissions, along with the reduction of using natural energy sources like fossil fuels [1]. The growth of renewable energy systems will enable the solutions of today's biggest issues, like enhancing the efficiency of organic fuels and the reliability of the energy supply. Promoting sustainable development in isolated desert and mountain areas and meeting the obligations of the nations involved. The establishment and execution of renewable energy projects in rural areas may reduce migration to cities by creating job opportunities [2].

According to the International Renewable Energy Agency (IRENA), renewable energy can and should supply 90% of the world's power by 2050 [3]. The smart grid combines and optimizes the usage of renewable energy, increasing the overall flexibility or dependability of the system while reducing energy dependency and improving energy security. The development of flexible power systems is not only an internal necessity to deal with diverse fault situations, but also an external drive caused by energy transition and technologies for smart grids [4]. This combination is important for developing a sustainable and clean energy system, which will provide us with a sustainable and resilient energy future.

Recent advancements in photovoltaic (PV) technology have led to solar energy prices approaching levels where it can effectively compete with widely used fossil fuel energy sources [5]. Recognizing the substantial energy potential of solar power, further progress is essential for solar energy to emerge as a significant contributor in the energy sector in the foreseeable future. The relationship between the power of a solar panel and its voltage reveals a Maximum Power Point (MPP), typically influenced by the solar light level. According to the maximum power transfer theorem, optimal power transfer occurs when the load resistance matches the panel's output resistance. achieving Maximum Power Point Tracking (MPPT) involves using a full-bridge DC-DC converter to match the load's resistance with the solar panel. The duty cycle, which is the ratio of the output voltage to the input voltage is the important parts in this process. This research aims to find the best method for the MPPT algorithm.

1.2 Problem Statement

Despite its widespread use and promising potential for energy with positive environmental impacts, the photovoltaic system encounters limitations in power generation efficiency and power transfer to the load. These limitations stem from various factors such as atmospheric temperature, solar radiation, module failures in the array, and a high ratio of shading among PV modules. This multiplicity poses challenges for the maximum power point tracking algorithm, potentially causing it to get stuck on local peaks and, consequently, leading to reduce power extraction from the PV array.

The MPPT control of a full-bridge microinverter in standalone photovoltaic applications encounters several challenges. Designing an effective MPPT control system involves addressing the trade-off between accuracy and complexity, with current methods potentially introducing intricacies and increased implementation costs, especially in small-scale and distributed photovoltaic systems. To optimize the highest power produced by the photovoltaic system under all operating conditions, an efficient tracking method is necessary. While some tracking algorithms exist for this purpose, they may not thoroughly search and compare all peaks in the P-V curve. In small and distributed PV systems, simplicity and cost-effectiveness are crucial, discouraging the preference for complex designs.

1.3 Objectives

The objective of this project:

i. To design the full-bridge DC-DC converter for microinverter application.

ii. To design and analyze the efficiency of MPPT controller for the full-bridge DC-DC converter.

iii. To simulate the integration of full bridge DC-DC converter with a single-phase H -bridge inverter.

1.4 Project Scope

The project's scope includes designing dual-stage microinverter and a full-bridge DC-DC converter using MATLAB/Simulink. The full-bridge DC-DC converter functions as the microinverter's first stage. A DC-AC converter has been integrated into the second stage, with a 500W power rating. The DC-AC inverter stage also makes use of an H-bridge inverter. The project also includes a comparative analysis of the microinverter's efficiency with a string inverter, providing a comprehensive exploration of the system's performance and functionality.

CHAPTER 2

LITERATURE REVIEW

2.1 Introduction

This literature review employs secondary data to provide a comprehensive summary of prior research relevant to the project's topic. The information will be gathered from diverse scholarly articles, journals, and other pertinent sources within the specific research domain. The utilization of secondary data allows for a thorough examination of existing knowledge, enabling the project to build upon and contribute to the broader body of research in the field. This approach ensures a robust foundation for the project by drawing on the insights, findings, and perspectives gleaned from previously conducted studies and scholarly works.

2.2 Renewable Energy Sources

Energy is the fundamental basis of the complex web of human activities that characterizes our contemporary lives. The two greatest issues the world is currently dealing with are climate change and increasing consumption of energy. Renewable energy sources will be very important to the world's future. There are three various types of energy resources such as fossil fuels, renewable resources, and nuclear resources [6]. Renewable energy sources, often called as an alternative form of energy, include biomass, geothermal, solar, wind, and other resources that can be utilized to generate energy again. When used for daily energy needs, renewable energy sources can provide power with little to no emissions of greenhouse gases and air pollution. [7].

One of the many advantages of renewable energy is its contribution to a more reliable and sustainable energy environment [8]. Its low impact on the environment is a key benefit, as it produces power with significantly fewer greenhouse gas emissions compared to conventional energy sources, thereby reducing the negative effects of climate change and air pollution. Another important advantage lies in the long-term viability of renewable resources, which provide a consistent and endless supply of energy through natural renewal. Utilizing energy from the sun, wind, and other renewable sources helps mitigate the negative effects of finite fossil fuel supplies while ensuring a steady flow of energy. The benefits of renewable energy are further highlighted in Table 2-1, which presents a comparison between non-renewable and renewable energy sources [9].

Table 2-1 : Comparison of Non-Renewable and Renewable Energy Sources

Criteria	Non-renewable Energy Resources	Renewable Energy Resources
Frequently used energy sources	One-time use	Reusable
Perpetual sources	Vanish one day	Available for perpetual use
Eco-friendly sources	Emits harm gases and pollute the environment	Does not emit gases and does not pollute the environment
Availability	Limited quantity	Unlimited quantity
Production cost	High	Low
Maintenance cost	Low	High
Production quantity	Large	Less

2.2.1 Solar Energy

Solar radiation is a form of electromagnetic radiation emitted by the sun, constitutes an abundant and fundamental energy source. This solar radiation, reaching every corner of the Earth over the course of a year, varies in intensity and duration depending on geographical location [10]. The dynamic interplay between the Earth's atmosphere, tilt, and orbit influences the amount of solar radiation received at any specific spot on the Earth's surface.

The Solar emits thermal and light energy, and photovoltaic solar cells convert into electrical and thermal energy [11]. Human beings have a difficult problem in developing sustainable energy supplies since the goal is to exceed demand for clean energy while reducing the world's reliance on fossil fuels. Solar energy is one of the most encouraging, long-lasting, universal, large-capacity, and ecologically benign renewable and sustainable energy sources. Despite the fact that natural sun irradiation is decentralized and discontinuous, solar energy use is widespread.

Solar energy is among the most dependable renewable energy sources and is mainly harnessed in two forms: photovoltaic (PV) power generation, which directly converts sunlight into electricity using the photovoltaic effect, and solar thermal energy, which focuses solar radiation to generate heat. This heat then drives a heat engine to produce electricity through thermal processes. Photovoltaic solar panels absorb solar radiation and are connected to a DC-to-DC converter, a DC to AC converter, a 3-phase line filter with transformer, and circuit breakers in order of operation in a photovoltaic solar energy conversion system. The system is controlled by a communication and control system. Before being transformed into utility-grade alternating current electricity, the generated power or converted energy can be stored in suitable thermal storage devices or batteries.

2.3 Characteristic of Photovoltaic Arrays

Solar panel installation can be either series or parallel depending on a number of important criteria, including output voltage and current. When several panels are arranged in series, their output voltages add up and their output current stays constant. In contrast, the output currents from multiple solar panels connected in parallel can be changes while the output voltages remain constant.

2.3.1 Series Connection

A power plant may occasionally need a system voltage much higher than what a single PV module can generate. In such cases, multiple PV modules (N-number) are connected in series to achieve the required voltage level. Just as cells are connected in series within a module, PV modules are similarly connected to attain the necessary voltage. This series wiring involves connecting the positive terminal of one panel to the negative terminal of the next panel. [12]. This configuration is ideal for unshaded conditions and when a low-amperage system is required, as it can use fewer cables and smaller gauge wires, making it more cost-effective. The benefits include easier maintenance without the need for additional equipment. However, a drawback is that in a series connection, each panel is crucial, if even one panel is shaded, the overall power output of the system declines. As shown in Figure 2-1, PV panels are connected in series.

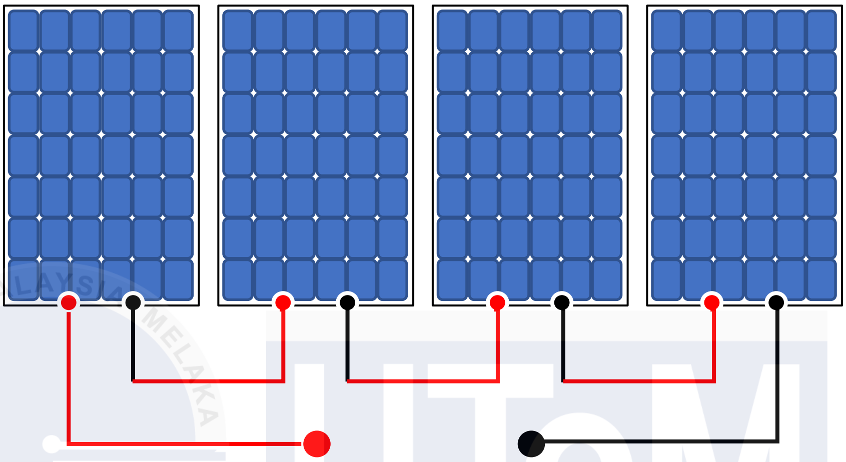

Figure 2-1 : PV panels in series connection

2.3.2 Parallel Connection

Usually, solar PV modules are connected in parallel instead of series to improve current instead of voltage while increasing the system's power. In a parallel combination of PV modules, the total current is the sum of the currents from each individual module. Since all the modules operate at the same voltage, the overall voltage in the parallel configuration remains equal to the voltage of a single module. This involves connecting the positive terminals of two panels together and the negative terminals of each panel together. Connecting in parallel allows your solar panels to produce energy without exceeding the operating voltage limit of the generator's inverter [13]. Solar panels in parallel operate independently of one another, making them the best option for mixed-light conditions, as they continue to work optimally even if one panel gets shaded. The advantages of this configuration include lower voltage levels, which reduce the risk of dangerous electrical conditions like arcing. However, a downside is that the increased amperage requires thicker and more expensive wires. Solar panels are connected in parallel as shown in Figure 2-2.

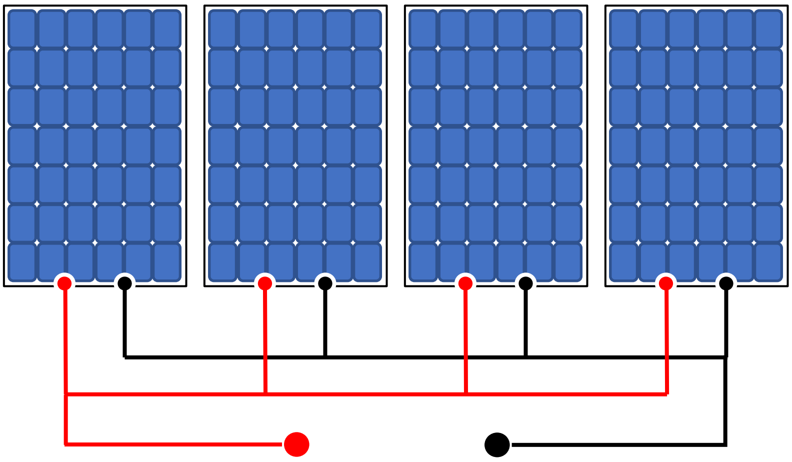

Figure 2-2 : PV panels in parallel connection

2.4 Maximum Power Point Tracking (MPPT) Controller

Effectively tracking solar power becomes challenging due to the nonlinear characteristics of the current-voltage (I-V) connection in photovoltaic (PV) panels, especially given the unique characteristics of the maximum power point (MPP) [14]. The MPP of the solar panel fluctuates due to atmospheric factors, such as solar radiation and cell temperature, which further complicate the situation. Consequently, it is essential to operate the PV panel at the voltage that correspondents with the MPP in order to maximize power generation. Achieving this criterion is the role of the maximum power point tracker (MPPT). Based on Figure 2-3, it shows the characteristics of P-V and I-V curve of the MPPT.

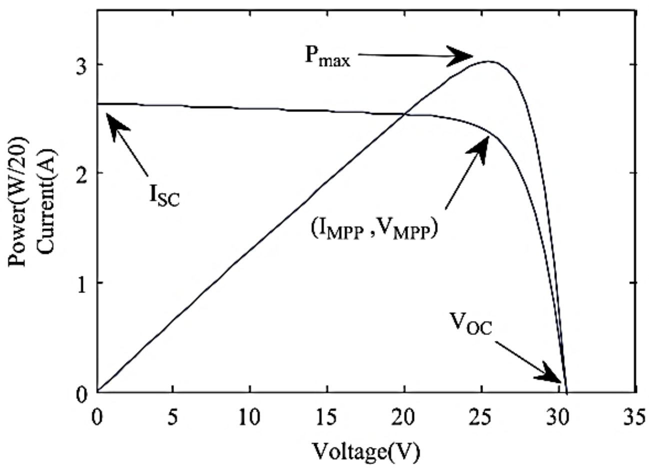

Figure 2-3 : P-V and I-V Curves [14]

While an MPPT is instrumental in obtaining the maximum power from a PV panel, it is considered an art due to the dynamic nature of the internal resistance of the PV panel under varying atmospheric conditions [15]. Despite the fluctuating internal resistance, the load resistance remains consistent. To address this, converters equipped with the MPPT algorithm come into play, ensuring load matching and maximizing power extraction from the PV panel.

To ensure the PV system operates close to the Maximum Power Point (MPP), a DC–DC converter with an MPPT controller is usually placed between the PV module and the load. Different MPPT algorithms, including short circuit, open circuit, ripple correction control (RCC), sliding mode control (SMC), perturb and observe (P&O), incremental conductance (IC), and fuzzy logic controller (FLC), have been studied in other research papers.

2.4.1 Perturb and Observe (P&O) Method

The P&O technique is distinguished as the most commonly utilized Maximum Power Point Tracking (MPPT) algorithm, employing a simple feedback configuration and a minimal set of measured parameters [15]. The module voltage experiences periodic disturbances, and the resultant output power is compared with the power observed in the previous perturbation cycle. A slight perturbation is introduced into the system, inducing variations in the power of the solar module. If the power increases due to the perturbation, the perturbation is sustained in the same direction. After reaching the peak power, where the power at the Maximum Power Point (MPP) is zero and subsequently decreases, the perturbation reverses [16]. As a stable condition is achieved, the algorithm oscillates around the peak power point, with the perturbation size deliberately kept very small to maintain minimal power variation.

Typically, in the P&O, a minor perturbation is introduced to cause power variations in the PV module. Periodic measurements of the PV output power are compared with the previous power, and if an increase is observed, the perturbation process continues, otherwise, it is reversed. Perturbations are applied to the PV module or array voltage, adjusting it to check for increases or decreases in power. When a voltage increases results in an increase in power, indicating that the PV module's operating point is to the left of the MPP, more disturbance is needed to move to the right in order to achieve the MPP. In contrast, if an increase in voltage results in a decrease in power, signifying that the operating point of the PV module is on the right of the MPP, further perturbation towards the left is needed to reach the MPP. Figure 2-4 shows the illustration of flowchart of P&O Method

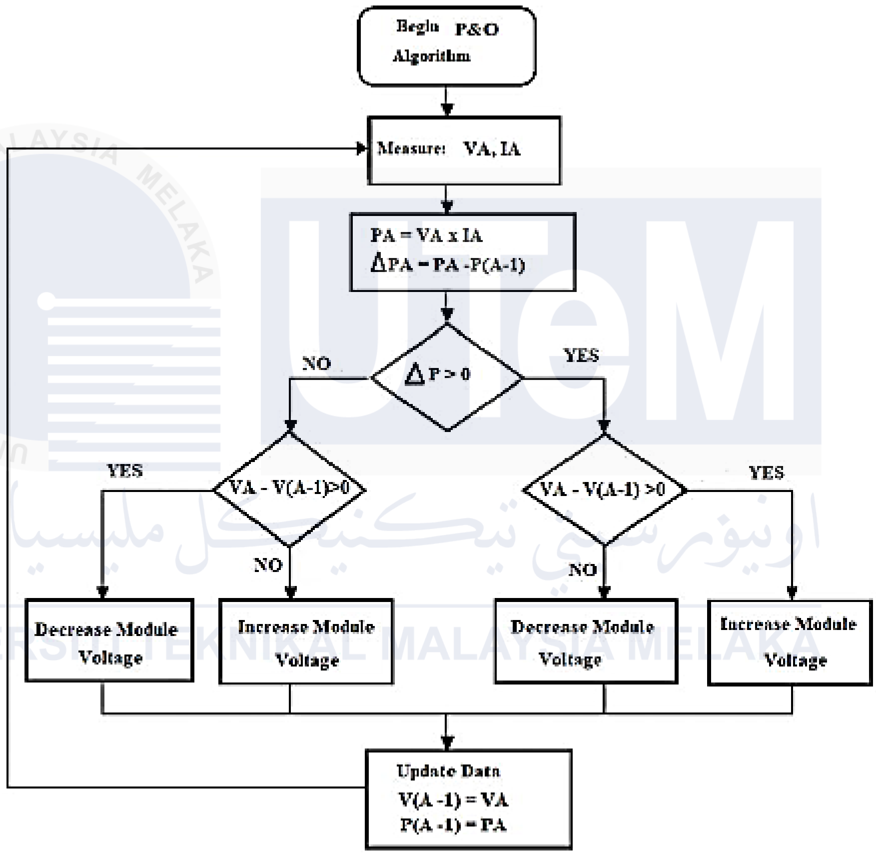

Figure 2-4 : Flowchart of P&O Method [16]

2.4.2 Incremental Conductance Method

The Incremental Conductance (IC) method addresses the limitations of the perturb and observe technique, particularly in effectively tracking peak power under rapidly changing atmospheric conditions [17]. Unlike the perturb and observe method, IC can identify when Maximum Power Point Tracking (MPPT) has achieved the Maximum Power Point (MPP) and stop adjusting the operating point accordingly.The relationship between $\frac{dI}{dV}$ and $\frac{-I}{V}$ can be applied to determine the direction in which the MPPT operating point should be perturbed if the condition is not satisfied.

This relationship is derived from the observation that $\frac{dP}{dV}$ is negative when the MPPT is on the right of the MPP and positive when it is on the left. Unlike the P&O method, which oscillates around the MPP, the IC algorithm reliably identifies when the MPPT has reached the MPP, presenting a clear advantage. Moreover, Incremental Conductance is more precise than the perturb and observe method in effectively monitoring quickly fluctuating irradiance conditions. [18].

However, it's important to note that the IC method is comparatively more complex than P&O. The basic idea is that the slope of P-V curve becomes zero at the MPP, as shown in Figure 2-5.

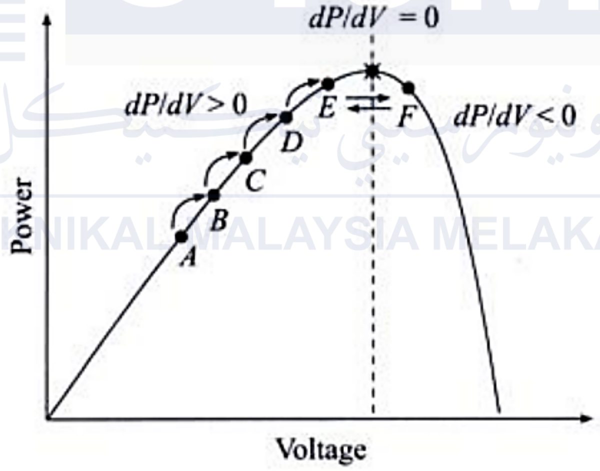

Figure 2-5 : Curve of IC Method [18]

2.5 DC-DC Converter

A DC-DC converter is a device that converts a direct current (DC) input's voltage level to a different DC voltage level. DC-DC converters can be categorized into two basic topologies, isolated and non-isolated [20]. In isolated DC-DC converters, the input and output are separated by an AC portion. These converters consist of an inverter to convert DC to AC, a transformer to adjust the AC voltage, and a rectifier to convert it back to DC. On the other hand, non-isolated DC converters directly convert DC input to DC output without AC isolation.

Examples of non-isolated DC-DC converters include the Buck, Boost, Buck-Boost, Cuk, and SEPIC converters. Example of isolated converters, are such as Push-pull, Forward, Flyback, Half-Bridge, and Full-Bridge converters, where it maintains separation between input and output through AC components. In non-isolated converters, a controlled switch is the key component responsible for the DC-DC conversion. When the switch is turned on, there is no voltage across the switch and the input voltage is observed across the load. Zero voltage is across the load and the entire input voltage is across the switch when the switch is off.

2.5.1 Forward Converter

A forward converter, categorized as a Switched-Mode Power Supply (SMPS), exhibits characteristics such as high output current, low ripple voltage, and a straightforward design. It is now widely used in computer and communication networks as a distributed power source [21]. Operating on the principle of stepping down voltage from input to output using a transformer, the forward converter, originating from the buck converter, maintains a basic and relatively simple structure. By modifying the transformer's turn ratio, it is able to increasing circuit voltage. The performance has improved and now have more topology options because of the recent improvements. However, this converter has two major drawbacks, transformer leakage inductance puts high voltage stress on the switch during switch shutdown, and energy trapped in the magnetizing inductance within the core causes transformer saturation [22].

The conventional forward converter consists of a power switch, either MOSFET or IGBT (S_1), three diodes (D_1, D_2, and D_3), a transformer (T_r), an inductor (L1), and two capacitors (C1 and C2). The output voltage (V_O) of the forward converter is directly related to the input voltage (V_{IN}), the turns ratio (n), and the duty cycle (D), as described by the following equation.

$$V_O = \left(\frac{N_2}{N_1}\right) D\ V_{IN} \tag{2.1}$$

The simplified circuit and associated voltage and current waveforms of Forward Converter are shown in Figure 2-6 and Figure 2-7.

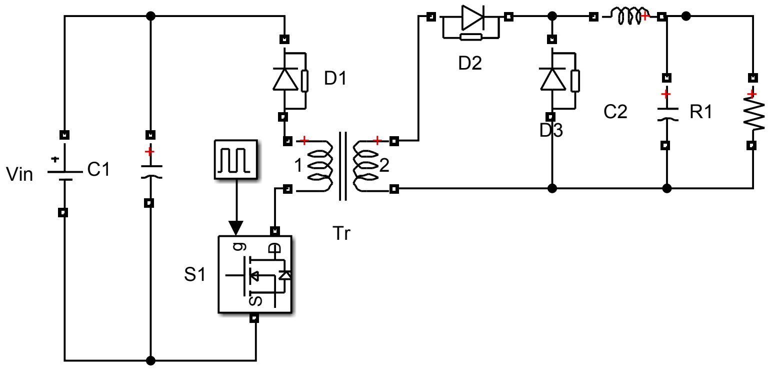

Figure 2-6 : Forward Converter

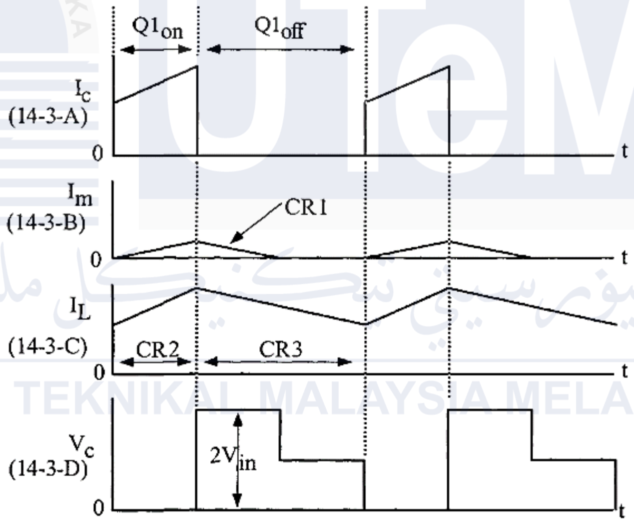

Figure 2-7 : Forward Converter Waveform [20]

2.5.2 Flyback Converter

Among isolated converters, the flyback converter stands out as the simplest. The flyback converter is a switched-mode power supply that is commonly used in low-power applications such as personal computers, LCD TVs, mobile phones, and notebook computers. Its applicability for low-power photovoltaic (PV) applications [23]. The flyback converter is unique because it can uses a coupled inductor instead of a regular transformer. However, this choice can result in higher leakage inductance.This high leakage inductance, in turn, causes substantial voltage spikes when the switch is turned off. Managing these voltage spikes is a crucial aspect of designing and optimizing the performance of flyback converters. Figure 2-8 shows the standard flyback converter comprises a power switch MOSFET or IGBT (S_1), a transformer (T_1), a diode (D_1), and a capacitor (C) and Figure 2-9 is the output waveform of flyback converter. The voltage gain expression in flyback configurations is formulated as follows:

$$G = \frac{V_o}{V_{in}} = n(\frac{D}{1 - D}) \tag{2.2}$$

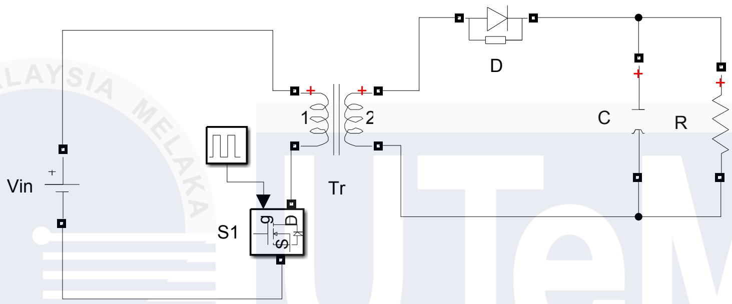

Figure 2-8 : Flyback Converter

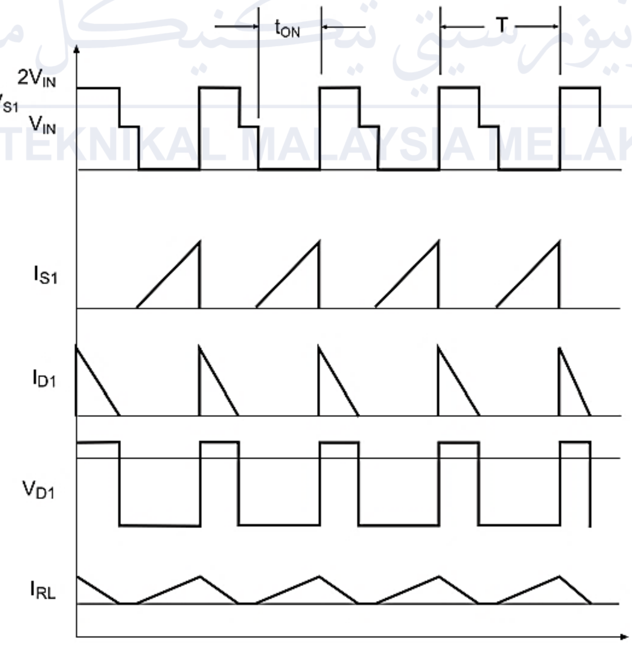

Figure 2-9 : Flyback Converter Waveform [22]

The flyback converter has various significant benefits. Firstly, it removes the requirement for a filter inductor in the output circuit. This is because the transformer secondary inductance functions in series with the diode while supplying current to the load. This unique characteristic makes the flyback converter well-suited for producing significant output voltages without needing a large filter inductor, typically used to reduce ripples in output currents.

2.5.3 Push-Pull Converter

Another type of DC-DC converter that have center-tapped transformer used in the primary and secondary windings circuit. This configuration allows for versatility in its applications, enabling it to function as either a step-up or step-down converter based on the turn ratios of the high-frequency transformer. Furthermore, the winding configuration of the high-frequency transformer allows for producing of different output voltages. The operation of a push-pull converter is the need to set the duty cycle to less than 50%, this is essential to prevent both switching devices from operating simultaneously, ensuring proper and controlled energy transfer through the transformer [24].

Due to its design and operational characteristics, the push-pull converter is suitable for medium-to-low power applications [25]. However, the presence of energy stored in the leakage inductances of the push-pull transformer can lead to complications. If no path is provided for this energy, voltage stress can occur on the semiconductor components, rendering the circuit impractical for use. Therefore, managing the energy stored in the leakage inductances becomes a critical aspect of the design and implementation of push-pull converters in practical applications. This challenge emphasizes the importance of careful consideration and design optimization to achieve efficient and reliable performance in real-world scenarios.

The push-pull configuration is a dual-ended topology where two transistors jointly handle the switching function. In this setup, the core of the transformer undergoes a complete swing in flux, fully optimizing its operation through symmetrical core activity the push-pull configuration consists of two switches, MOSFET or IGBT (S_1 and S_2), a transformer with a center-tapped (T_1), two diodes (D_1 and D_2), and one LC filter. Figure 2-10 and Figure 2-11 illustrates the circuit and waveforms associated with this arrangement. The output voltage (V_o) is proportional to the input voltage (V_{in}), the turns ratio (n), and the duty cycle (D), as shown in the following equation:

$$V_o = 2n(V_{in})(D) \tag{2.3}$$

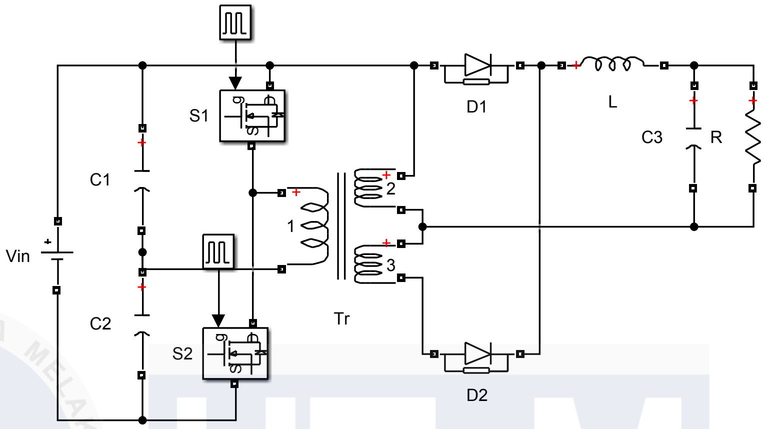

Figure 2-10 : Push-Pull Converter

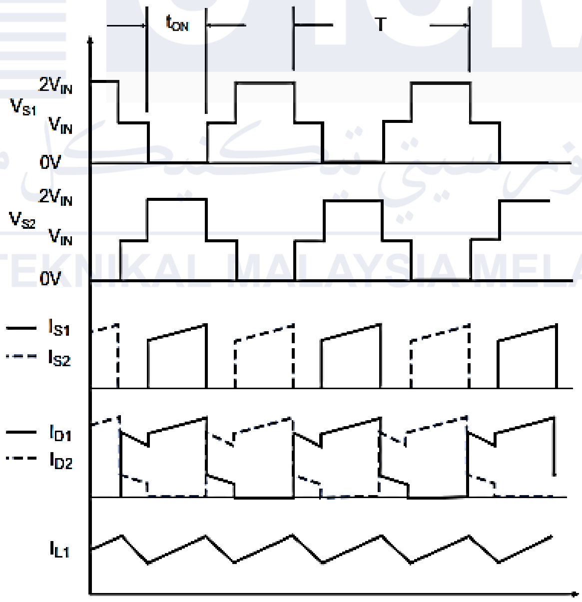

Figure 2-11 : Push-Pull Converter Waveform [22]

The push-pull topology facilitates a compact design of the transformer and output filter, resulting in very low output ripple. Each switch operates with nearly a 45% duty ratio, contributing to an exceptionally high operating frequency of 90% for the converter's total switching frequency [26]. Consequently, push-pull converters are well-suited for high power density and low ripple outputs. However, the push-pull topology is also having some disadvantages. Each transistor in the converter needs to handle twice the input voltage because of the doubling effect caused by the center-tapped primary winding. Additionally, practical considerations prevent the two halves of the winding and the two power switches from being perfectly identical, leading to flux symmetry imbalances.

2.5.4 Half-Bridge Converter

Half-bridge converters can be utilized in applications with power ratings up to 500 W, benefiting from their simplified structure with fewer switching elements. In comparison to full-bridge configurations, the reduced number of switching elements leads to lower switching losses [27]. In the context of DC-DC conversion with the ability to supply output voltages higher or lower than the input voltage while providing isolation through a transformer. When comparing it to flyback and forward converters, the half-bridge stands out for its potential to yield higher output power while utilizing smaller and less expensive components.

In the half-bridge topology, both switches must operate with the same pulse width. This ensure that the midpoint between capacitors C1 and C2 is maintained at half of the input DC voltage. Figure 2-12 depicts the circuit configurations of the half-bridge converter. The filtering capacitor serve as voltage dividers, resulting in a $\frac{\text{Vin}}{2}$ applied voltage across each primary winding.

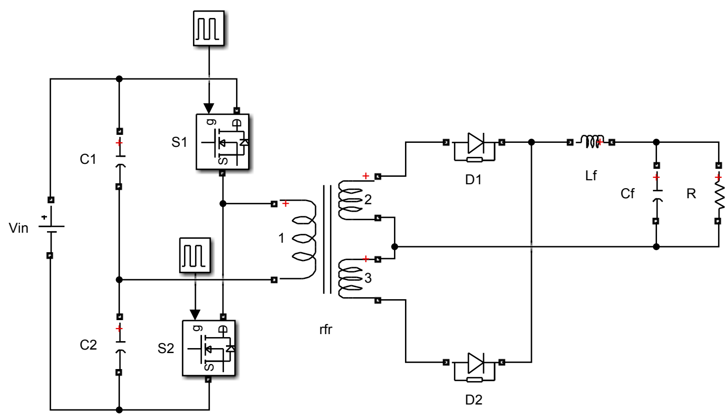

Figure 2-12 : Half-Bridge Converter

Switching dynamics are managed such that S_1 and S_2 operate in a complementary fashion with equal conduction periods, preventing a short circuit of the input voltage. A duty ratio of less than 50% is obtained from the dead period in which both switches are off. Figure 2-13 shows fundamental waveforms for current and voltage of Half-Bridge Converter.

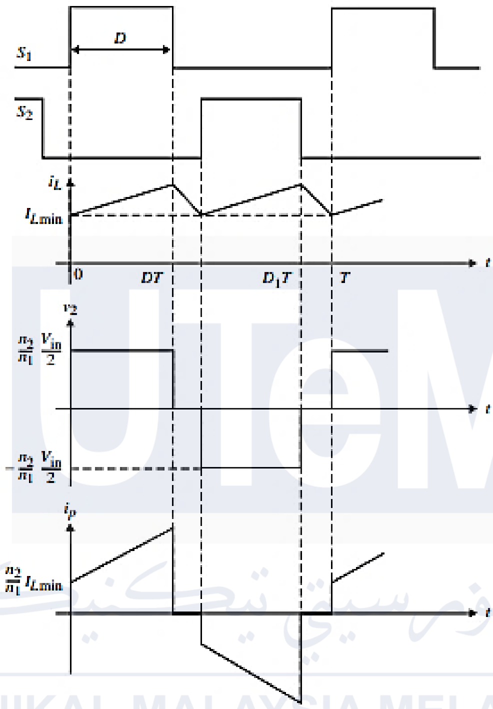

Figure 2-13 : Waveform of Half-Bridge Converter [27]

The voltage gains of the half-bridge converter mirrors that of the push-pull converter, and filtering capacitors C_1 and C_2 divide the input voltage, each carrying $\frac{\text{Vin}}{2}$. Significantly, in the half-bridge converter, each switch is designed to handle a maximum blocking voltage of Vout, unlike the push-pull configuration, where it is 2Vin.

2.5.5 Full-Bridge Converter

The full-bridge converter is a highly versatile and commonly selected topology, particularly favored for high-voltage and high-power systems where enhanced efficiency and dependability are critical considerations. Its ability to handle substantial electrical power levels makes it well-suited for applications demanding high voltage and power [28]. The basic topology of a full-bridge converter is as shown in Figure 2-14 where it consists of a high-frequency transformer and Figure 2-15 the output waveform of the Full-Bridge Converter. The full-bridge configuration comprises four power switches, either MOSFETs or IGBTs (S_1, S_2, S_3, S_4), on the primary side of the transformer (T_1). Meanwhile, the secondary side of the transformer incorporates two diodes (D_1, D_2), an inductor (L), and an output capacitor (C). The output voltage (V_o) of this converter is determined by the following formula:

$$V_o = 2V_{in}(D)\left(\frac{N_S}{N_P}\right) \tag{2.4}$$

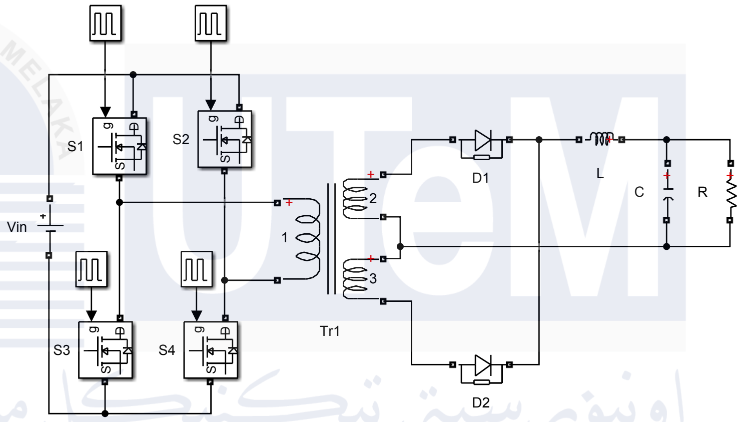

Figure 2-14 : Full-Bridge Converter

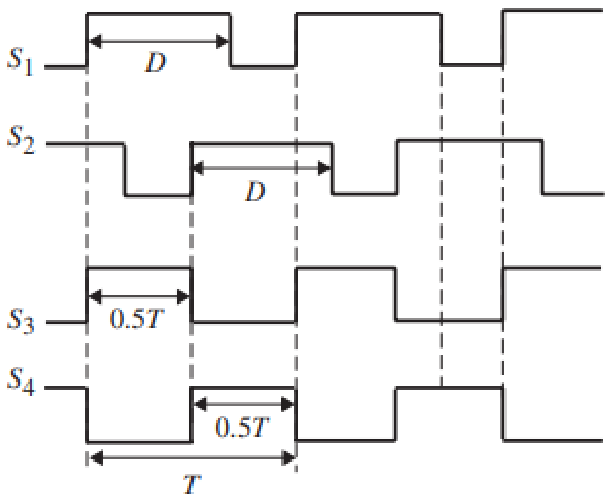

Figure 2-15 : Full-Bridge Converter Waveform [28]

The full-bridge converter stands out due to its versatility, making it suitable for a wide range of applications, from low-power, low-voltage systems to high-power, high-voltage systems. This versatility contributes to its widespread use in various industries, providing an effective solution for diverse power requirements. One of the full-bridge converter's primary characteristics is its efficiency in power conversion. This efficiency is very valuable for circumstances were reducing energy losses and ensuring maintaining optimal performance and utilization of resources. The full-bridge converter's configuration, utilizing a bridge with four switching devices, enables bidirectional energy flow and effective control of the output voltage. This control, often achieved through pulse-width modulation (PWM) techniques, allows for precise regulation of the output, contributing to its suitability for different applications.

The applications of the full-bridge converter are diverse, ranging from power supplies for industrial equipment to renewable energy systems and high-power electronic devices. In high-voltage and high-power scenarios, reliability is paramount, and the full-bridge converter, when appropriately designed and implemented, offers a dependable solution. Its reliability, coupled with its adaptability and efficiency, makes the full-bridge converter a preferred choice for addressing the complex power demands of modern systems across various industries.

2.6 Inverter

The primary role of solar inverters is to transform the direct current (DC) generated by solar panels into the alternating current (AC) utilized in households. There are two primary categories of residential solar inverters, which are microinverter and string inverter.

i. Microinverters mounted on the back of each panel are ideal for complex solar configurations, converting direct current (DC) from individual PV modules into alternating current (AC). The AC electricity generated by each microinverter is consolidated into a single output and fed into the utility grid. These inverters typically range in capacity from 250W to 400W [30].

ii. String inverters link arrays of panels to a central location and are optimal for straightforward installations. When a string of PV solar modules is connected to a single inverter, the alternating current power generated from each string inverter is combined into a single output and then transmitted to the utility grid. The capacity of this inverter ranges from 2kW to 30kW [30].

Figure 2-16 shows the comparison of installation arrangement between String Inverter and Microinverter.

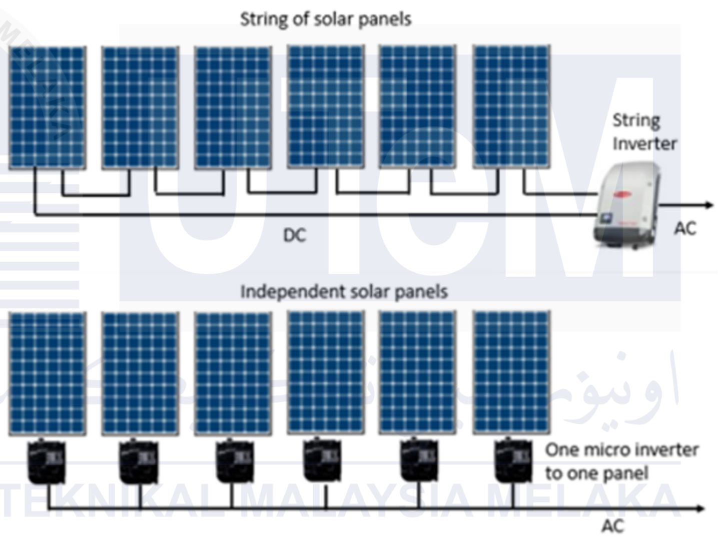

Figure 2-16 : Comparison between String Inverter and Microinveter [29]

2.6.1 String Inverter

A string inverter is commonly placed near the main service panel or electric meter in a residential setting. They connect strings of solar panels in one central location, making them suitable for straightforward installations. In a string configuration, several panels are connected in series, forming a string. These inverters handle the DC output from multiple interconnected panels and convert it into usable AC energy for everyday use. One advantage of string inverters is their ability to handle multiple strings of panels attached to them. However, there are trade-offs. While they are easy to troubleshoot (since no one needs to climb onto the roof for repairs), they have a critical limitation: if there is an issue with one panel in the string (such as shading or failure), it affects the entire string's energy production. Unlike microinverters, which allow each panel to operate independently, string inverters rely on the performance of the entire string. Figure 2-17 shows how the arrangement panel for string inverter.

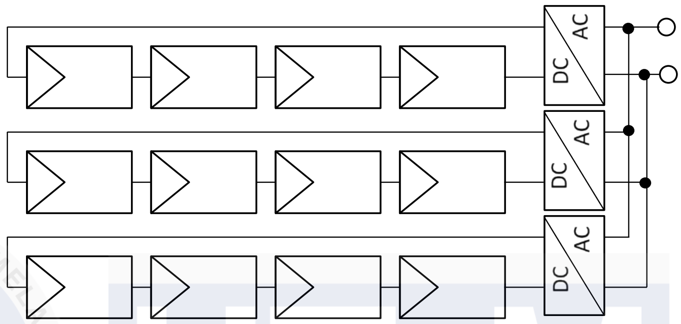

Figure 2-17 : String Inverter configuration

To address shading issues and maximize energy production, string inverters are often paired with DC power optimizers [31]. These optimizers enhance efficiency by optimizing the performance of individual panels. Additionally, string inverters have a medium power rating (up to 5 kW) and better efficiency compared to central inverters. Maintenance requirements for string inverters are lower than those for central inverters. They are suitable for medium to large solar systems and can operate in either single-phase or three-phase configurations. Each string has its dedicated inverter, allowing for better control and monitoring of the entire solar system. However, installation costs tend to be higher due to their multiple-unit setup.

Issues with one panel in a string can affect the energy production of the entire interconnected set due to the wiring configuration of the solar panels. For example, if a panel in the string is shaded and produces less energy, all other panels in the same string will match the output of that shaded panel. String inverters are commonly used in residential solar setups because they simplify installation on unshaded roofs. To meet electrical code standards, string inverters are often paired with DC power optimizers. These optimizers, mounted on the back of each panel, monitor peak output, regulate voltage before it reaches the string inverter, optimize energy production, and mitigate the effects of shading. Figure 2-18 illustrates a typical setup for a residential solar system utilizing string inverters and DC optimizers.

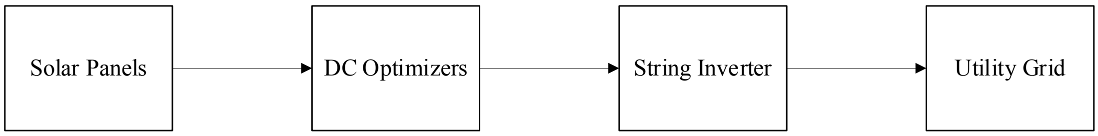

Figure 2-18 : Residential Solar System with String Inverter and DC Optimizers

2.6.2 Microinverter

A microinverter is a compact device installed under an individual PV panel and connected in parallel with other microinverters in an array. When integrated with a PV panel before installation, this combination is often referred to as an AC module [30]. Despite its smaller size, a microinverter performs the same essential functions as a central inverter, efficiently converting DC to grid-synced AC, preventing system islanding, optimizing efficiency through MPPT.

Additionally, shading on a single module affects only that module's performance, rather than the entire string. Second, microinverters offer higher efficiency compared to central and string inverters. They also have a low maintenance cost and are suitable for small-scale installations. However, it's worth noting that their installation cost tends to be higher than both central and string inverters. Moreover, microinverters typically operate in single-phase systems. Overall, they provide a reliable and efficient way to convert solar energy into usable electricity. The installation of microinverters enhances power generation efficiency from the same number of panels. Figure 2-18 shows the arrangement for microinverter configuration.

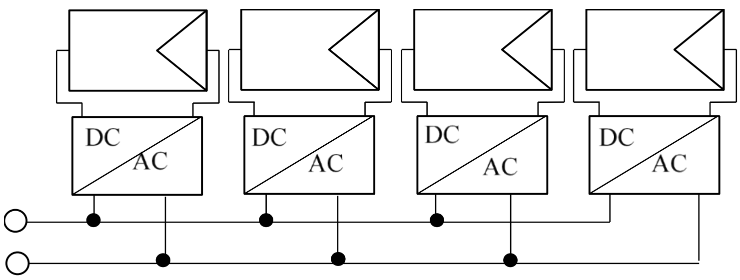

Figure 2-19 : Microinverter configuration

Table 2-2 presents the comparison of commonly used inverters in solar power systems, including central inverters, string inverters, and microinverters

Table 2-2 : Comparison of Inverter

Parameters	Central Inverter	String Inverter	Microinverter
Shading effect	Partial shading on a single module will affect overall performance.	Shading on one module will impact the performance of the entire string of modules.	Shading on a single module will affect the performance of that module alone.
Power rating	High power rating which is more than 2kW	Medium power rating which is up to 5kW	Low power rating which is up to 400W
Efficiency	Average	Better than central inverter	Higher than central and string
Maintenance	High	Less than central	Very low
Scale	Large	Medium to large	Small
Phases	3-phase	1 phase/ 3 phase	1 phase
Inverter arrangement	Single inverter for all modules	Inverter attached to each string	Inverter attached to each module
Installation cost	Low	More than central	Higher than both
Maintenance cost	High	Less than central	Very low

2.6.3 Full-Bridge Inverter

The full bridge topology, depicted in Figure 2-20, consists of four switching devices, with two devices situated on each leg. This full-bridge inverter has the capability to generate twice the output power of a half-bridge inverter with an equivalent input voltage. A zero-sequence voltage is added to the modulation signals to ensure that the devices are clamped either to the positive or negative DC rail. This process improves voltage gain, resulting in an elevated load fundamental voltage, diminished total current distortion, and an increased load power factor [34]. The top devices are designated as S_{11} and S_{21}, while the bottom devices are denoted as S_{12} and S_{22}. The voltage equations for this converter are provided in the subsequent equations.

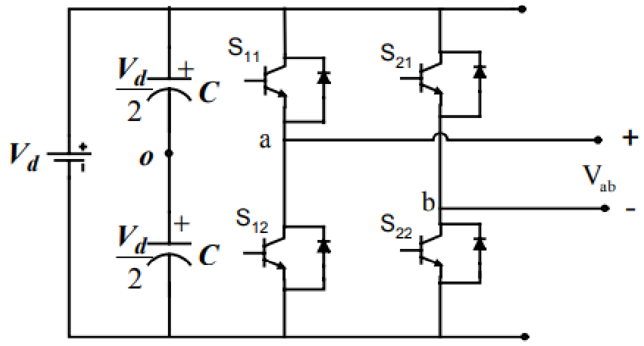

Figure 2-20 : Full-Bridge Inverter [34]

$$\frac{V_d}{2}(S_{11} - S_{12}) = V_{an} + V_{no} = V_{ao} \tag{2.5}$$

$$\frac{V_d}{2}(S_{21} - S_{22}) = V_{bn} + V_{no} = V_{bo} \tag{2.6}$$

$$V_{an} - V_{bn} = V_{ab} \tag{2.7}$$

The voltages, denoted as V, represent the output voltages from phases A and B to a designated point, labeled as n. V represents the neutral voltage between point n and the midpoint of the DC source. The switching behavior of the devices can be estimated using a Fourier series, expressed as $\frac{1}{2}(1+M)$ where M is the modulation signal. When compared to the triangular waveform, this modulation signal determines the switching pulses.

2.7 Photovoltaic Application

Photovoltaic systems can be broadly divided into two primary categories:

i. On-grid systems, where photovoltaic systems are connected to the public electricity network.

ii. Standalone systems (off-grid), which are photovoltaic systems not connected to the network.

Additionally, there are various subtypes of photovoltaic systems based on factors such as their type, method of connection to the network, or the approach to storing energy in independent systems.

2.7.1 Grid Connected PV System

A grid-connected photovoltaic power system is a setup for generating electricity that is linked to the utility grid. A power conditioning unit (PCU), a number of inverters, solar panels, and grid connection hardware are commonly included in this system. The grid-connected photovoltaic system feeds the extra energy that exceeds the linked load's consumption back into the utility grid when the circumstances are right. Figure 2-21 illustrate the basic block diagram of PV grid-connected system.

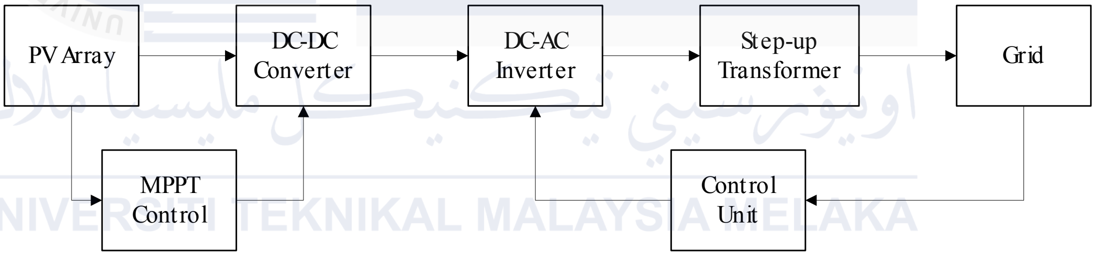

Figure 2-21 : Block diagram of PV Grid-Connected System

In the grid-connected system, it is integrated with a sizable public electrical grid owned by a utility company, contributing generated power to the overall grid. These systems vary in scale, ranging from residential setups (2-10 kW) to larger solar power stations (1-10 MW) [35]. Grid-connected photovoltaic systems installed in homes or buildings fulfil the structure's electrical needs where any excess power will be transferred into the grid when it becomes available.

An example of an existing real-life application is the Enphase Microinverter, which exemplifies advanced features that enhance solar energy production [37]. Specifically designed to maximize energy output from solar module arrays, the Enphase Microinverter demonstrates efficiency in renewable energy systems. In operational configurations, each Enphase Microinverter seamlessly integrates into a 3-phase system by automatically connecting to one of the phases, showcasing intelligent functionality for easy deployment within larger electrical networks. By sensing and synchronizing with the grid and designated phase, the microinverter ensures harmonious interaction with existing power infrastructure. Enphase Microinverters are typically deployed in groups of three for optimal performance, contributing to the stability and efficiency of the electrical distribution network. Figure 2-22 shows an example of an Enphase microinverter.

Figure 2-22 : Enphase IQ8M Microinverter [37]

2.7.2 Standalone PV System

An off-grid or Standalone PV System is comprised of individual photovoltaic modules (or panels), typically 12 volts each, with power outputs ranging between 50 and 100+ watts. These PV modules are combined into a unified array to meet the desired power requirements. A basic standalone PV system is an automated solar system designed to generate electrical power, charging banks of batteries during daylight hours for later use when solar energy is not available. Small-scale stand-alone PV systems utilize rechargeable batteries to store the electrical energy produced by PV panels or arrays [36]. These systems are well-suited for remote rural areas and scenarios where alternative power sources are either impractical or unavailable for supplying power to lighting, appliances, and other needs. In such situations, it is more cost-effective to install a standalone PV system than to incur the expenses of extending power lines from the local electricity company directly to the location, as would be done in a grid-connected PV system.

Conductors, electrical components, one or more loads, and one or more photovoltaic (PV) modules constitute an electrical system which is a standalone PV system. It's worth noting that, in the case of small-scale off-grid solar applications, building structures or rooftops need not be the permanent home of the solar system. Off-grid solar systems are widely used to power isolated sites such as camper vans, recreational vehicles, boats, tents, and camping settings. Figure 2-23 shows the block diagram of standalone PV system.

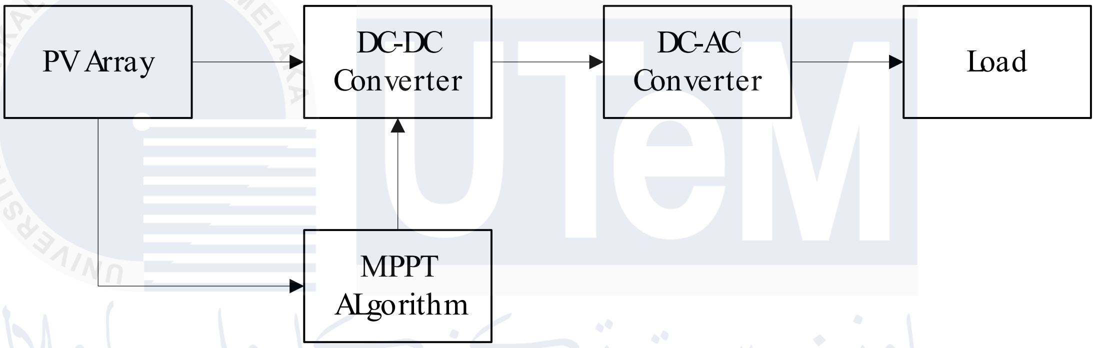

Figure 2-23 : Block Diagram of Standalone System

As the existing real-life, the successfully developed and implemented a standalone PV microinverter, integrating it into the innovative Solar Kiosk by UM Power Energy Dedicated Advanced Centre (UMPEDAC) [38] . This achievement marks a significant step forward in the application of microinverters for standalone photovoltaic systems. The Solar Kiosk, with its integrated microinverter technology, holds promise for diverse applications, potentially replacing conventional caravans or generators in various settings. One of the key advantages of the Solar Kiosk lies in its contribution to a green environment. Unlike traditional generators, which often emit harmful pollutants, this solar-powered kiosk operates without generating air and noise pollution. This environmental-friendly feature makes the Solar Kiosk a sustainable and responsible choice for power generation.

Moreover, the Solar Kiosk offers a practical solution for extended electricity consumption. With approximately seven (7) hours of free electricity consumption, it addresses the energy needs of users, particularly in off-grid or remote areas. This aspect enhances the accessibility and affordability of electricity, contributing to the socio-economic development of communities. In terms of construction, the Solar Kiosk is designed with durability in mind. Its structure is crafted from fiber-reinforced plastic (RFP) materials, ensuring resilience against various environmental conditions. This choice of materials not only enhances the kiosk's longevity but also showcases a commitment to using sustainable and robust components.

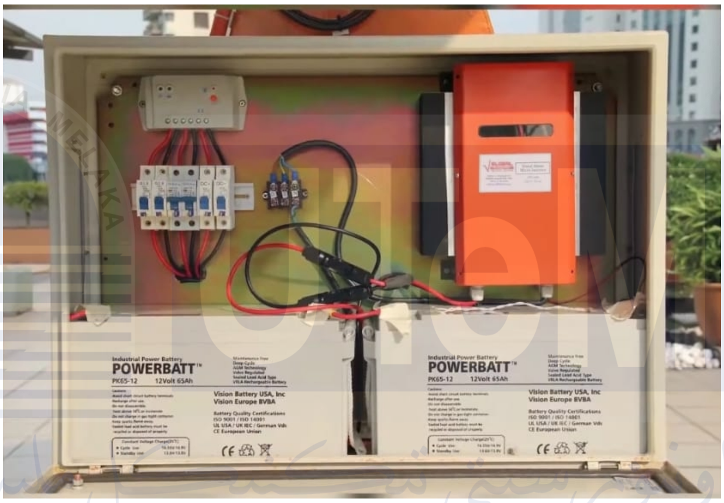

Figure 2-24 : Solar Kiosk [38]

2.8 Summary

The literature review on "MPPT Control of Full-Bridge Microinverter for Standalone Photovoltaic Application" covers solar energy's role in renewable energy and the characteristics of photovoltaic (PV) arrays in series and parallel configurations. It examines Maximum Power Point Tracking (MPPT) techniques, especially Perturb and Observe and Incremental Conductance, for optimizing PV efficiency. The review evaluates various DC-DC converters, including Forward, Flyback, Push-Pull, Half-Bridge, and Full-Bridge converters. It compares string inverters and microinverters, highlighting the advantages of microinverters for standalone PV systems. Moreover, it compares grid-connected and standalone PV applications, with an emphasis on standalone systems relevant to the thesis.

CHAPTER 3

METHODOLOGY

3.1 Introduction of methodology

In this methodology chapter, two studies are presented, which were focusing on the isolated full bridge DC-DC converter and microinverter circuit design. It is essential to note that these studies represent separate designs and not connected with each other. The formula use is a general that applicable to converter design, and its comprehensive discussion, along with the detailed exploration of the design. Both the converter and inverter designs were implemented using MATLAB/SIMULINK, providing a practical dimension to the discussed methodologies. The chapter aims to fully clarify the design approach and the implementation of the chosen formula in both conditions, providing a thorough understanding of the study.

3.2 Methodology of the project

The methodology of this project revolves around investigating the performance of a converter in the context of microinverter applications. The primary aim is to comprehensively study and evaluate the converter's effectiveness within this specific application. To achieve this, the project draws upon existing research papers as references. The implementation involves conducting simulations for both the converter and inverter, providing a practical and insightful examination of their performance characteristics. Through this methodology, the project aims to contribute valuable insights into the functionality and efficiency of converters in the microinverter context, leveraging simulation techniques for a thorough analysis.

3.3 Flowchart of the project

Figure 3-1 illustrates the flowchart of the research activity conducted for this project. By reviewing past literature and studies, the design for converter and inverter can be set. If the performance is not satisfied yet these parameters can be adjusted to achieve the desired outcome.

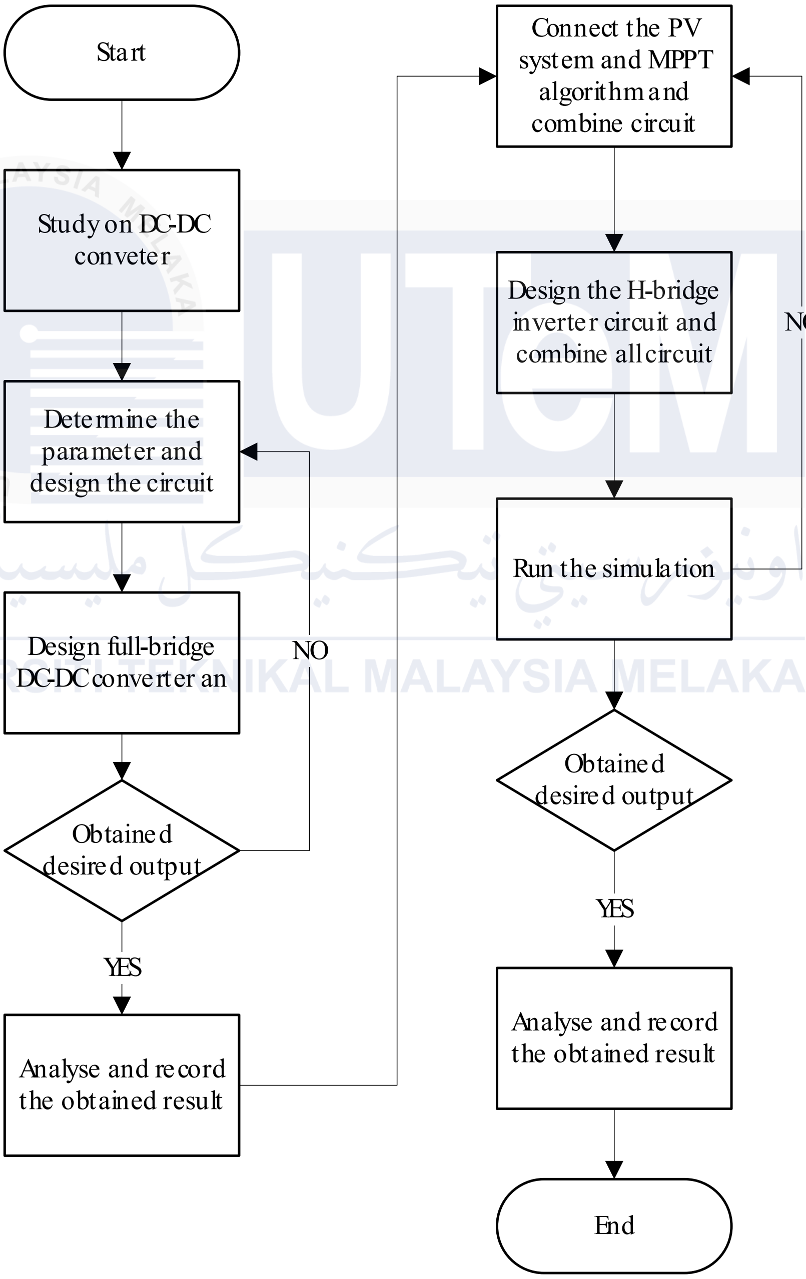

Figure 3-1 : Flowchart of the project

3.4 Flowchart of DC-DC converter design

Figure 3-2 shows the flowchart for designing the Full-Bridge Converter. It includes with calculating and setting component values and also deciding on the switching control values. Then, the circuit is designed in MATLAB/Simulink.

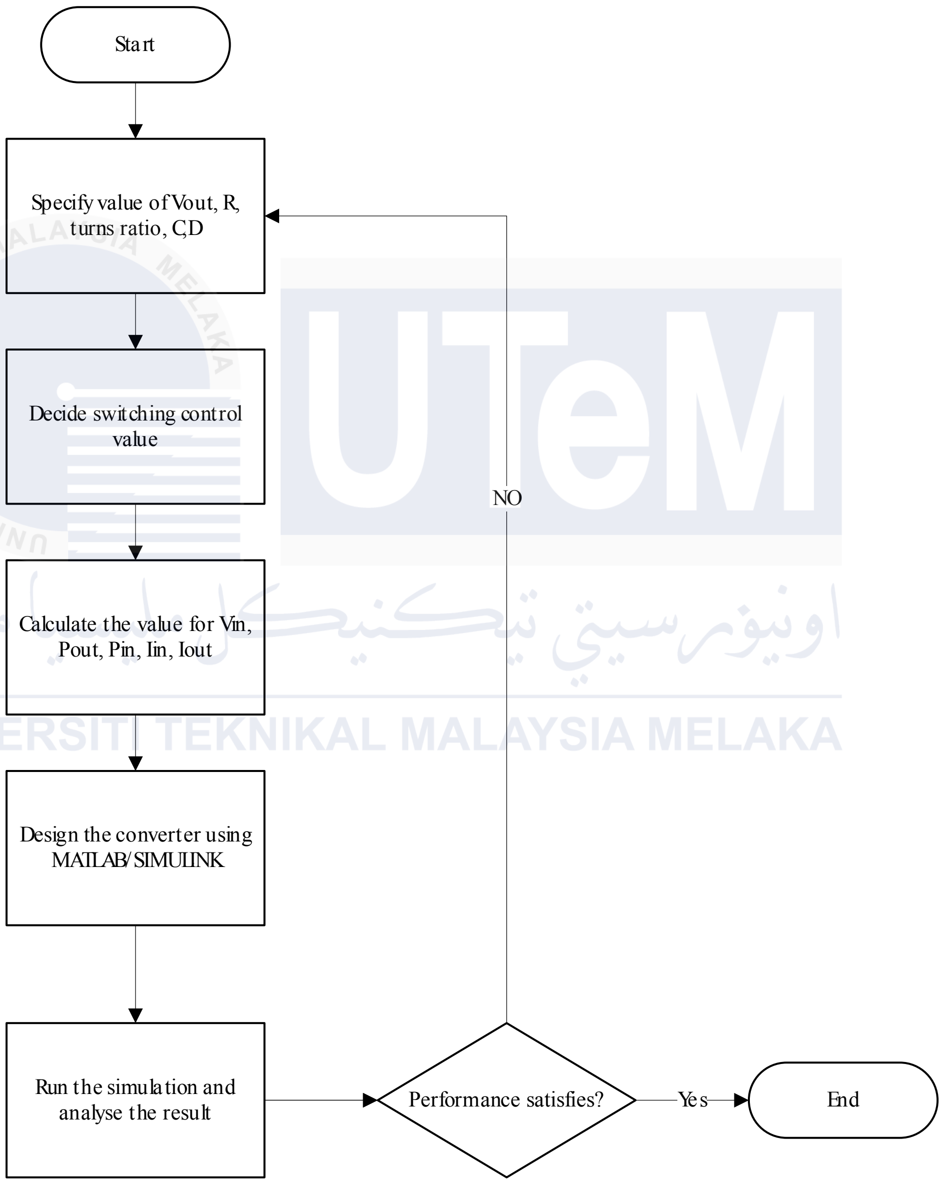

Figure 3-2 : Flowchart for Converter Design

3.5 Flowchart of Microinverter Design

Figure 3-3 shows the flowchart for designing the microinverter. The process involves specifying component values, designing the H-bridge inverter, and integrating it with the full-bridge converter.

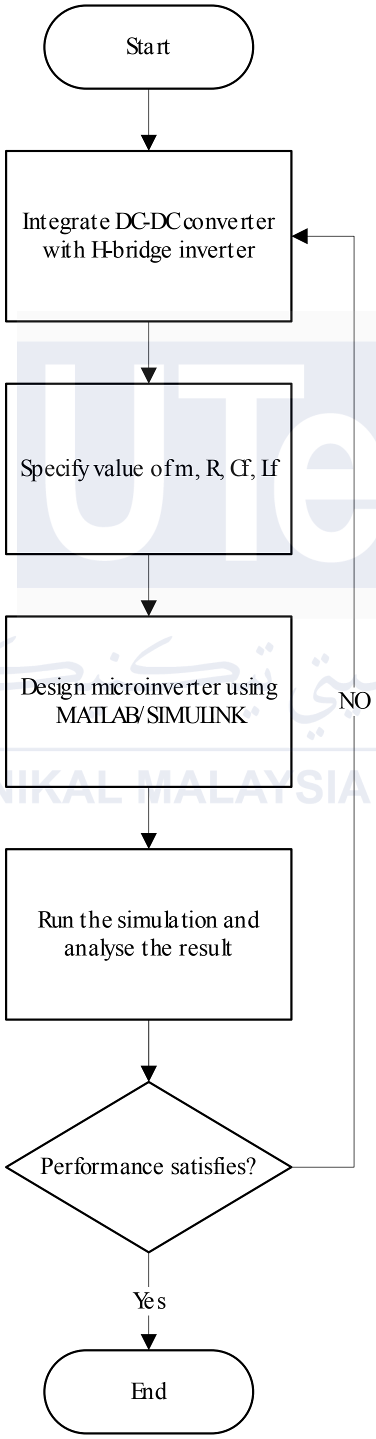

Figure 3-3 : Flowchart for Microinverter Design

3.6 Design of Full-Bridge DC-DC Converter

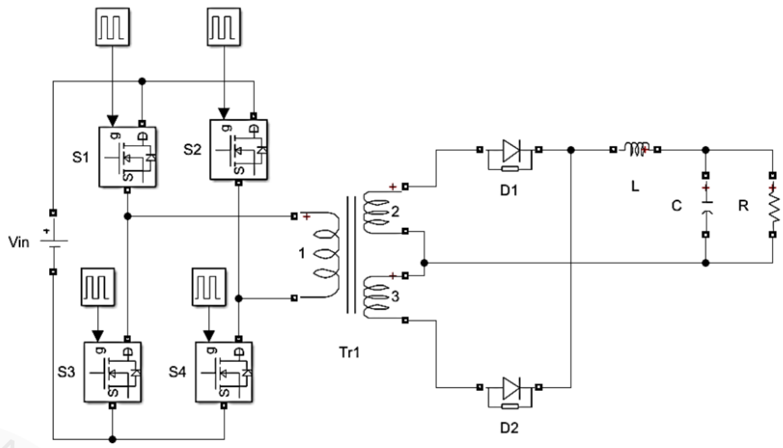

Figure 3-4 : Design of Full-Bridge DC-DC Converter

The DC-DC converter is a full bridge isolated phase shifted converter as shown in Figure 3-4. In order to transfer electricity from the primary side to the secondary side, a full bridge takes place when two of the four switches are paired and turned on. By using soft switching in the phase shift type, efficiency is increased.

The MOSFET's ON-resistance is low when S_1 and S_4 are turned on, this can be seen as a short circuit between the source and the drain. S_2 and S_3 are in the OFF state as a result of the voltage Vin being applied between the MOSFET's drain and source. V_{in} is also applied to S_1 and S_4 when they are in the OFF state, in along with S_2 and S_3.

Mode 1: When S_1 and S_4 are turned on

When triggering S_1 and S_4, V_{in} is positively applied to the primary transformer's dot end. By now, the diode D_1 is forward biased, causing the dot end of the secondary side to become positive and ON. Soft switching is used at the beginning of this period because there is no voltage between the source and the drain. Also, the capacitor, C is charged. That takes some time to switch to OFF.

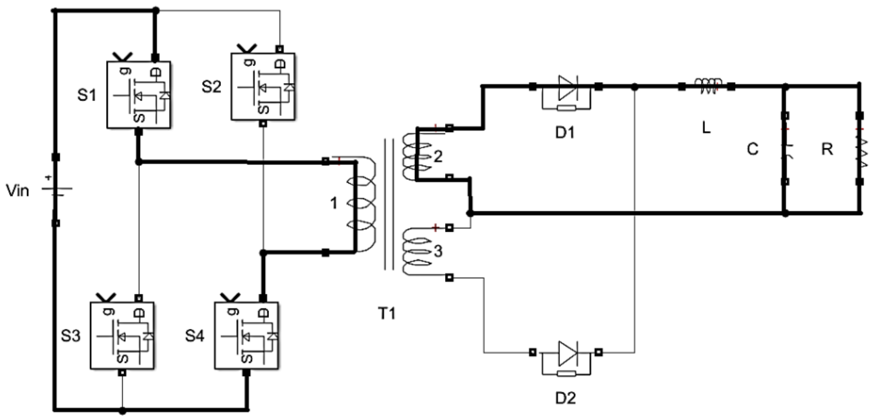

Figure 3-5 : Operation Mode 1

Mode 2: When S_2 and S_3 are turned on

When S_2 and S_3 are turned ON, there is no voltage between S_2's drain and source, and soft switching is accomplished. Both the primary and secondary sides of the transformer become positive. Electric power flows from the primary to the secondary side when D_1 is turned ON to charge the capacitor C.

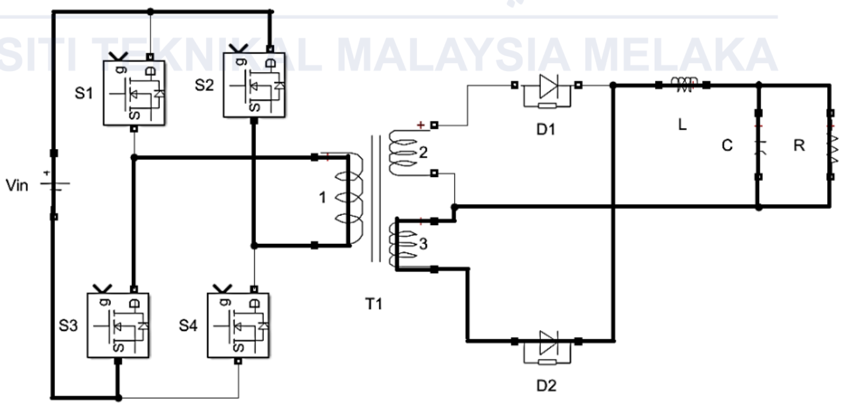

Figure 3-6 : Operation Mode 2

3.7 Simulation setup for full-bridge DC-DC converter

The center-tapped transformer, inductor, capacitor and power switches are important elements of the full bridge converter design. The full-bridge DC-DC converter can be implemented properly based on these designs. The entire specification of the proposed bridge converter is shown below:

The output voltage of full-bridge DC-DC converter:

$$V_O = 2V_{in}(\frac{N_S}{N_P})D \tag{3.1}$$

During switch S_1 and S_4 closed

$$V_P = V_{in} \tag{3.2}$$

Where;

$$V_{S1,2} = V_{in}(\frac{N_S}{N_P}) \tag{3.3}$$

$$V_{P2} = V_{in} \tag{3.4}$$

During switch S_1 and S_4 closed

$$V_{P2} = -V_{in} \tag{3.5}$$

Where;

$$V_{P1} = -V_{in} \tag{3.6}$$

$$V_{S1,2} = -V_{in}(\frac{N_S}{N_P}) \tag{3.7}$$

$$V_{S1} = 2V_{in} \tag{3.8}$$

The turn ratio can be determined by;

$$\frac{N_P}{N_S} = 2\left(\frac{V_{in}}{V_O}\right)D \tag{3.9}$$

The selected inductance value can be expressed through;

$$L_x = \frac{V_O(0.5 - D)}{\Delta i_x\, f} \tag{3.10}$$

Where;

$$I_{Lx} = \frac{V_o}{R} \tag{3.11}$$

$$\Delta_{ix} = 0.4\, I_{Lx} \tag{3.12}$$

The selected capacitor value can be expressed through;

$$\frac{\Delta V_O}{V_O} = \frac{1 - 2D}{32\, f^2\, L_X\, C} \tag{3.13}$$

3.8 Implementation design of full-bridge DC-DC converter

This is the basic setup for full-bridge DC-DC converter design. The function for this converter is to convert a DC voltage to a different and providing a regulated output. Switched mode DC-DC converters, commonly known as switching power supplies are the category in which the circuits discussed. This discussion focuses on achieving an output voltage of 400V and a power output of 500W. Figure 3-7 illustrates the circuit of a basic full-bridge DC-DC converter. Before the transformer, four MOSFETs are used to generate sinusoidal pulse width modulation (SPWM). The transformer employed is a step-up transformer with a ratio of 1:2.

The proposed full-bridge converter specification is given below

-Output Voltage, V_O: 400V

-Input Voltage, V_{in}: 200V

-Output Power: 500W

-Number of turns ratio, $\frac{N_1}{N_2}$ = 1:2

i) Find the duty ratio from the expected output voltage

$$Vo = 2V_S(\frac{N_S}{N_P})D$$

$$400 = 2(200)\left(\frac{2}{1}\right)D$$

$$D = 0.5$$

ii) Find the secondary winding voltage

$$V_{s1,s2} = V_{in}(\frac{N_S}{N_P})$$

$$V_{S1,S2} = 200\left(\frac{2}{1}\right)$$

$$V_{S1,S2} = 400$$

iii) Find the voltage at primary winding

$$V_p = V_{in}$$

$$V_p = 200$$

iv) Find the value of inductance

$$I_{LX} = \frac{V_o}{R} = \frac{400}{200k} = 20mH$$

$$\Delta_{ix} = 0.4I_{LX} = 0.4(20m) = 0.8mH$$

$$L_X = \frac{400(0.5 - 0.8)}{0.8m\ (5k)} = 30H$$

v) Find the value of capacitor

Assuming ripple 5%

$$\frac{\Delta V_o}{V_O} = \frac{1 - 2D}{32(f^2)L_X C}$$

$$0.05 = \frac{1 - 2(0.8)}{32(5k^2)(30)\ C}$$

C = 0.5nF

Table 3-1 : Parameter for Full-Bridge DC-DC Converter Circuit

Parameters	Value
Vin	200 V
Vout	397.9 V
Duty cycle, D	0.7
Switching frequency	2kHz
Turn ratio	1:2
Capacitor, C	10µF
Inductor, L	10mH

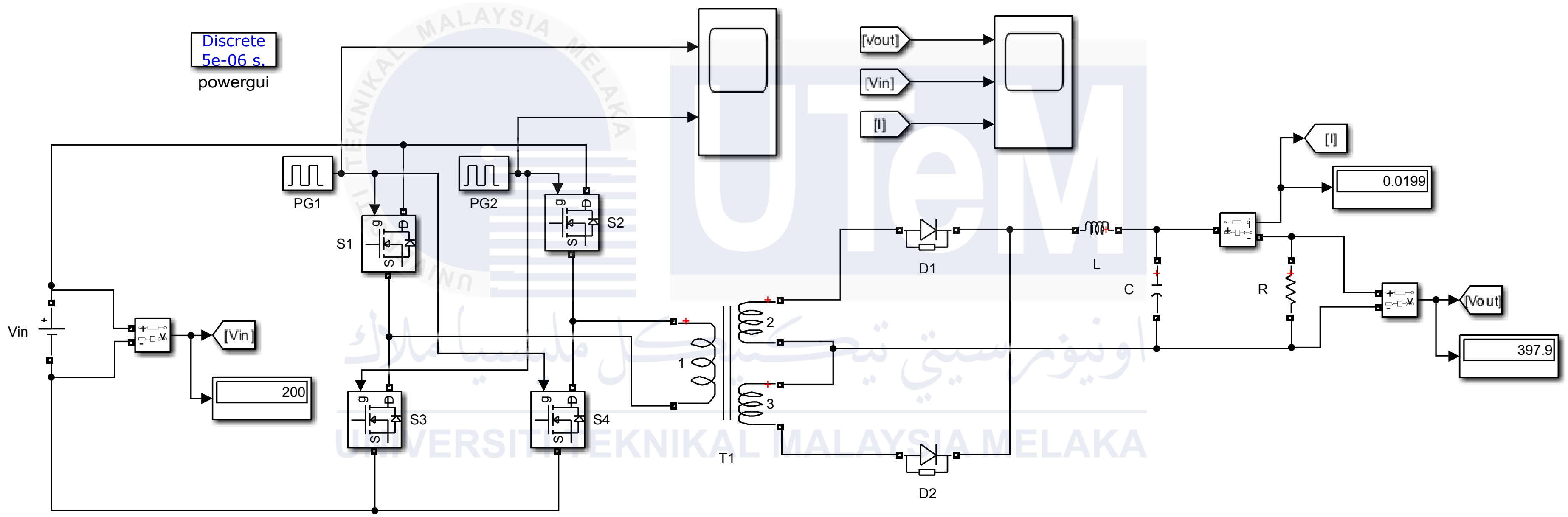

Figure 3-7 : Full-Bridge DC-DC Converter Circuit

3.9 Design for full-bridge PV microinverter

The full-bridge DC-DC converter has been configured to utilize a photovoltaic (PV) panel as its primary input source, replacing the DC source. Specifically, the chosen PV panel model is the Grape Solar GS-S-405 Platinum. To enhance its efficiency, the PV panel is set up with a configuration of 1 series and 2 parallel connections. Figure 3-10 presents an illustration of the circuit simulation developed by integrating the PV source with the full-bridge DC-DC converter. In this arrangement, the Perturb and Observe (P&O) method is used as an algorithm to regulate the pulse width modulation (PWM) signals transmitted to the full-bridge converter circuit. These PWM signals are generated by a PWM generator block and then routed to the suitable MOSFETs within the circuit. This method helps to make sure the power conversion works well with the PV panel's specific features.

3.9.1 Grape Solar GS-S-405 Platinum

The specifications for the selected PV panel, Grape Solar GS-S-405 Platinum, are tabulated in Table 3-2. In the MATLAB/Simulink simulation, this parameter from Table 3-2 is applied. These properties provide important information on the solar cells or photovoltaic panel's characteristics, particularly how its voltage and current respond to different operating conditions and temperature changes. The voltage between the terminals of a circuit when no load is attached is known as the open circuit voltage (Voc). 60.38 volts is the open circuit voltage in this data. Short-circuit current is the highest current that may flow through a device when its terminal is immediately shorted (Isc). This solar panel has a measured 8.66A for short circuit current. The voltage at the maximum power point (Vmp), which is 50.06 volts according to the data, is the voltage at which the device operates with the highest output of power. (Imp), or the operating current at the maximum point, is 8.1A in the data. The open circuit voltage's (Voc) temperature coefficient illustrates how the Voc changes with temperature. As the temperature rises, the open-circuit voltage is seen to decrease by -0.36779% for each degree Celsius. The temperature dependence of the short-circuit current (Isc) is displayed by the Isc temperature coefficient. As the temperature rises, it increases by 0.043995% for every degree Celsius. The figure 3-8 illustrates the I-V characteristics for Grape Solar GS-S-405-Platinum while Figure 3-9 illustrates the P-V characteristics based on the configuration for 1 parallel panel and 2 series panel. Figure 3-10 illustrates the circuit full-bridge PV converter.

Table 3-2 : Photovoltaic PV Panel Parameters

Parameters	Value
Open-circuit voltage, V_{OC}	60.38V
Short-circuit voltage, Isc	8.66A
Voltage at maximum point, Vmp	50.06V
Current at maximum point, Imp	8.1A
Temperature coefficient of Voc	-0.36779 %/deg.C
Temperature coefficient of Isc	0.043995 %/deg.C

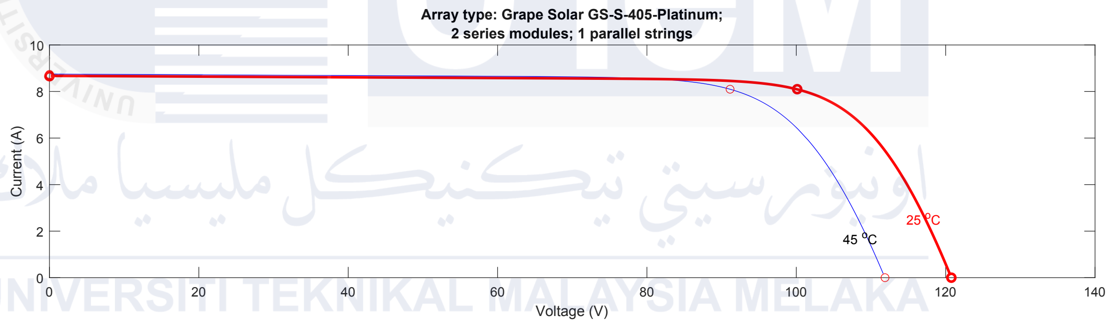

Figure 3-8 : I-V characteristics

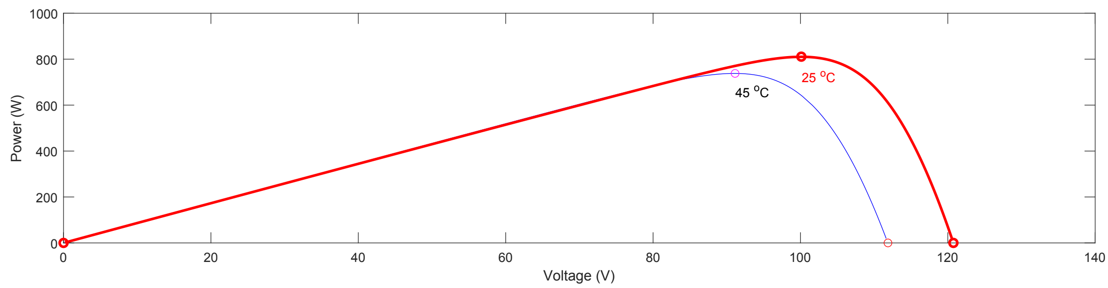

Figure 3-9 : P-V characteristics

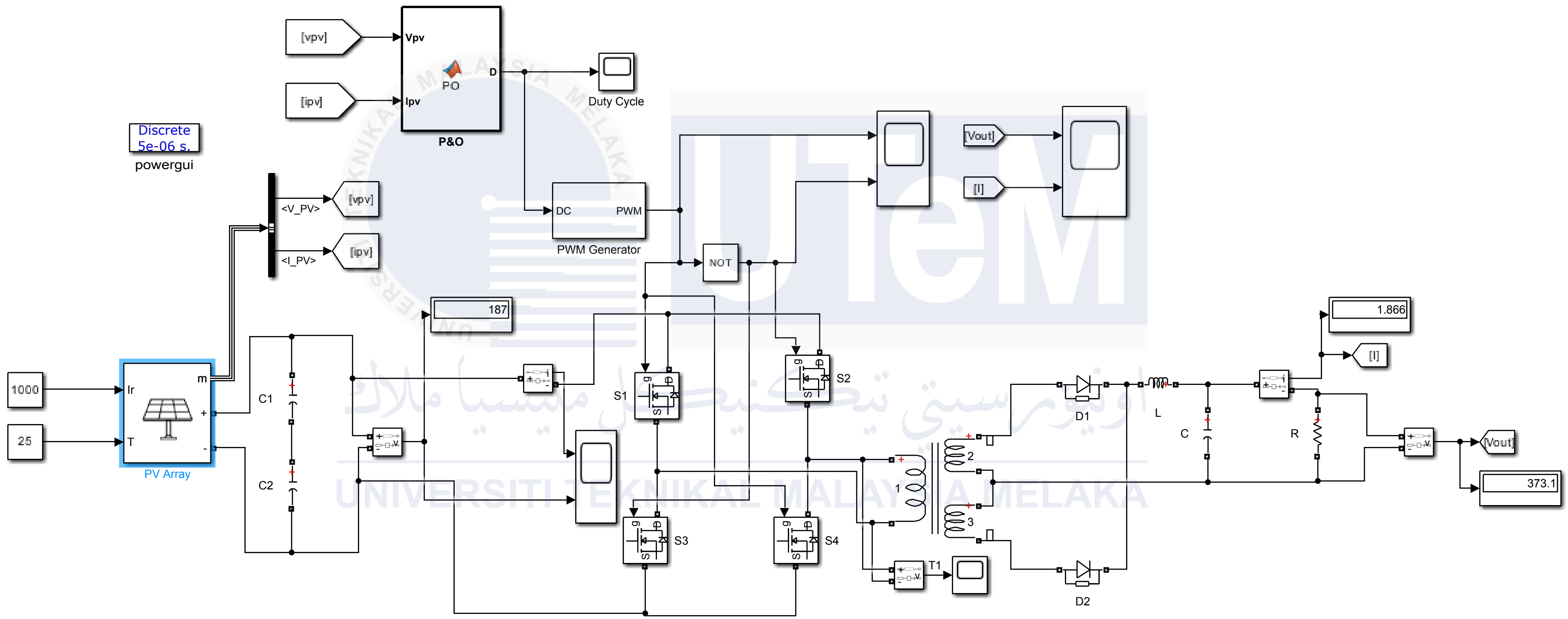

Figure 3-10 : Full-Bridge PV Circuit

3.10 Design for single-phase H-bridge inverter

The load is connected at the center points of the two legs of an h-bridge inverter, which has two legs with two switches each. Consider the h-bridge circuit as shown in Figure 3-11 uses 4 MOSFET. The H-Bridge receives power from DC source Vdc. There are three alternative ways to switch the switches S1, S2, S3, and S4. When S1 and S2 are turned on, the output produces +Vdc. When S3 and S4 are turned on, the output produces -Vdc. When S1 and S2 or S3 and S4 are turned on simultaneously, the output voltage is zero.

Mode 1: S1 & S4 Turn ON

The output of a bipolar PWM inverter alternate between +Vdc and -Vdc. When the amplitude of the sinusoidal control signal is greater than the amplitude of the triangular carrier signal, switches S1 and S4 turn on and switches S2 and S3 turn off. At this moment, if the load current i_o is in a positive direction, S1 and S4 will be turned on as shown in Figure 3-11.

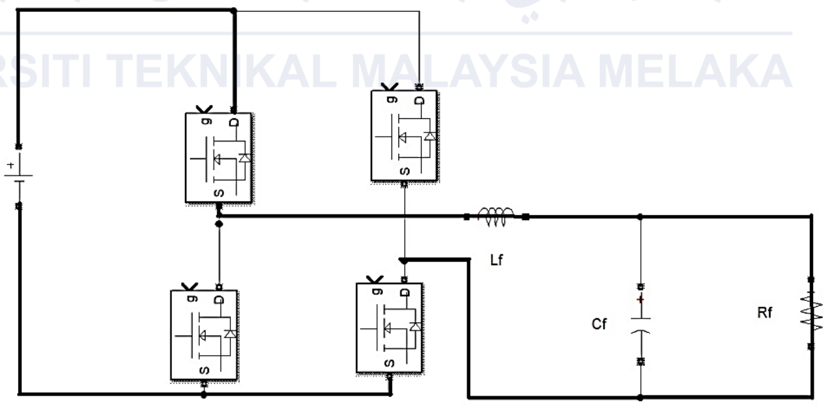

Figure 3-11 : Operation Mode 1

Mode 2: S2 & S3 Turn ON

In operating mode 2, when the amplitude of the triangular carrier signal is greater than the amplitude of the sinusoidal control signal, switches S2 and S3 turn on and switches S1 and S4 turn off. At this moment, if the load current i_o is in a negative direction, S2 and S3 will be turned on as shown in Figure 3-12.

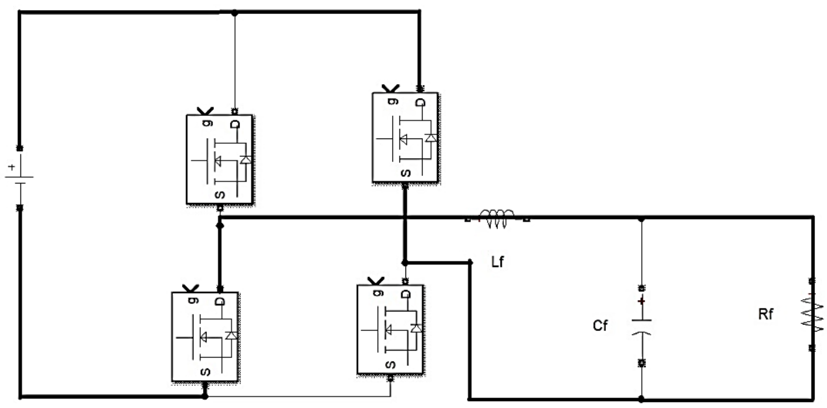

Figure 3-12 : Operation Mode 2

3.11 Simulation setup for H-Bridge Inverter

The parameters required for designing an H-bridge inverter, as displayed in Table 3-3. Understanding these parameters is vital for achieving optimal performance and efficiency in inverter design. The input voltage for this H-bridge inverter design is set at 400V. This high input voltage is to ensures that the inverter can meet the demands of high-power applications and providing a stable power supply for various loads. The modulation index (Ma) is set to 0.6. This ratio determines the amplitude of the output AC waveform relative to the input voltage. By setting Ma to 0.6, the inverter's output voltage is 60% of the input voltage, resulting in a peak output voltage of 230Vrms. A higher switching frequency improves the smoothness of the output waveform but also increases switching losses and thermal stress on the MOSFETs. A 50µF capacitor filter (Cf) is used to reduce voltage ripple and provide a stable DC voltage. This stabilization improves the reliability and efficiency of the inverter. An inductor filter (Lf) is connected to enhance the power factor and smooth the current waveform. This integration helps reduce harmonic distortion and produces a more sinusoidal current. A load resistor (R) of 200 kilo-ohms is connected in parallel with other loads in the circuit. This resistor simulates real-world load conditions and ensures that the inverter can handle multiple loads simultaneously, maintaining stability and performance. Understanding and optimizing these parameters are essential steps in achieving a reliable and high-performance H-bridge inverter design.

Table 3-3: H-bridge Inverter Parameter

Parameters	Value
Vin	400V
Modulation amplitude, Ma	0.8
Switching frequency	2kHz
Capacitor, CF	30µF
Inductor, LF	20mH
Resistive load	100Ω

3.11.1 Bipolar Switching

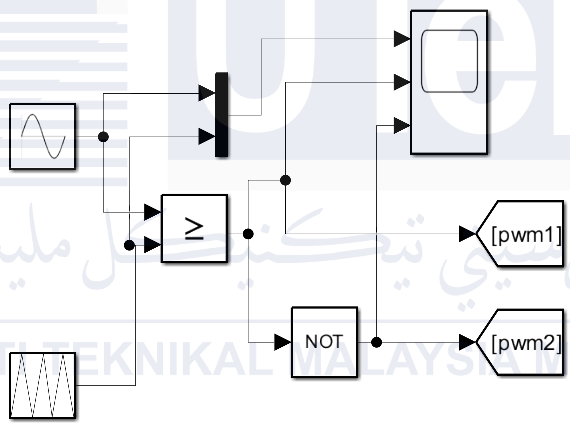

Figure 3-13 : PWM Switching

When one switch is switched on while the other is off, the upper and lower switches in the same inverter leg function in a complementary way. As a result, we only need to take into account the two separate gating signals, V_{g1} and V_{g3}, which are produced by contrasting the sinusoidal modulating wave, V_m and the triangular carrier wave, V_{cr}. The inverter output voltage $V_{AB} = V_{AN} - V_{BN}$ and the inverter terminal voltages V_{AN} and V_{BN} are obtained. Bipolar PWM is the name given to this system because the waveform of the VAB alternates between positive and negative dc voltages [39]. Figure 3-13 illustrates the PWM switching for H-bridge inverter.

Figure 3-14 show the output for switching bipolar PWM. The operation of a bipolar PWM inverter involves alternating the output between positive and negative Vdc voltages based on the comparison of a sinusoidal control signal with a triangular carrier signal.

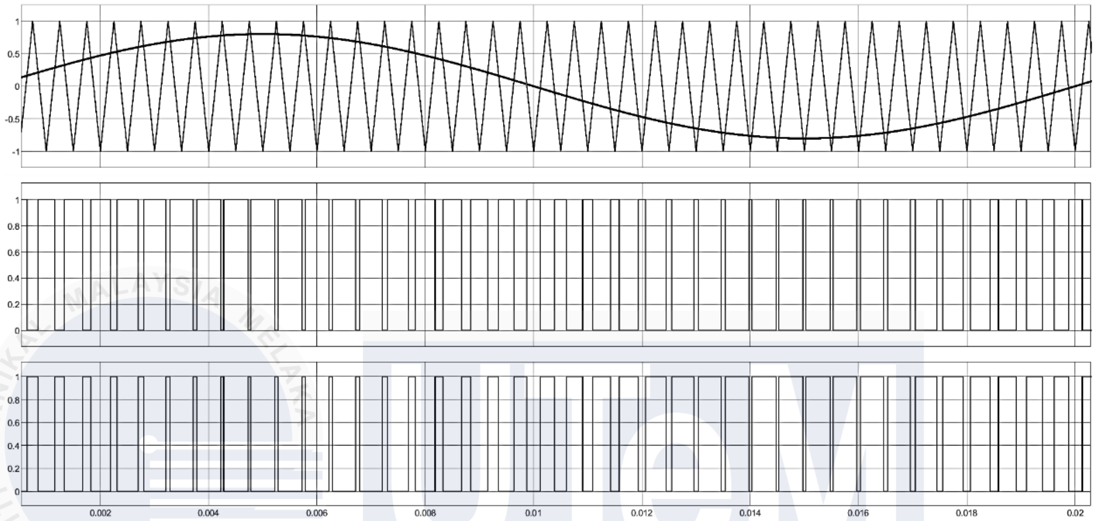

Figure 3-14 : Bipolar PWM Switching

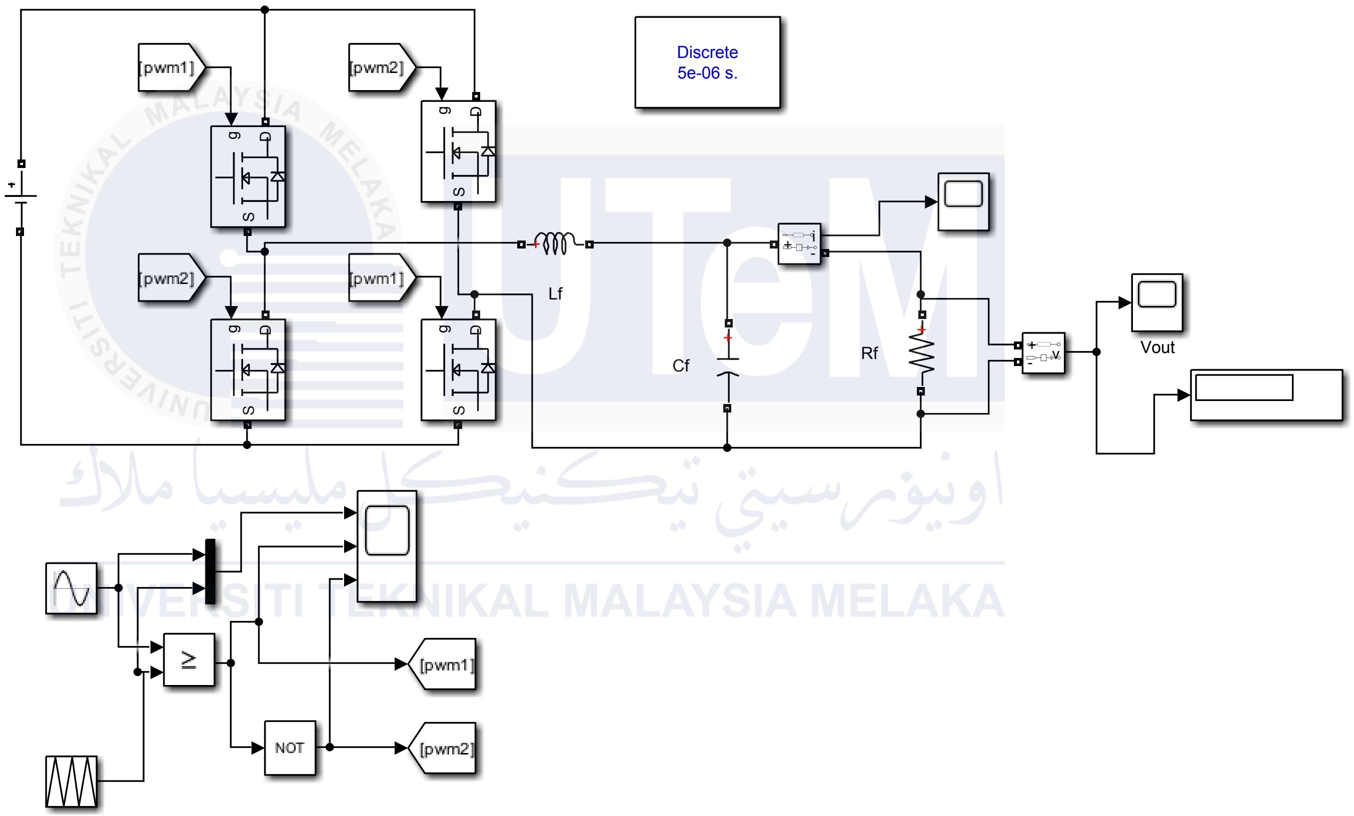

Figure 3-15: Single phase H-bridge Inverter Circuit

3.12 Design for dual-stage Full-Bridge Microinverter

The design for the dual-stage full-bridge microinverter, as illustrated in Figure 3-12, can be divided into three main components which are the MPPT and PV side, the full-bridge converter, and the inverter. In order to successfully transform the power from a photovoltaic (PV) panel to a functional AC output, each of these parts is important.

The PV side and MPPT (Maximum Power Point Tracking) serve as the first part. By continually adjusting the voltage at the operating point of the modules or array in order to achieve maximum power extraction, MPPT is in charge of maximizing the power output from the PV panel. On the PV side, direct current (DC) power is first generated and must be transformed into the appropriate voltage levels in order to be used further. The second part is the full-bridge converter. In this part, the DC power from the PV panels is converted to a higher DC voltage using a full-bridge configuration. A transformer with a 1:4 turns ratio is used to step up the input voltage from 115V to an output voltage of 400V, which is essential for achieving the necessary voltage levels for subsequent stages. A pulse generator is used to create the control signals for the MOSFETs in the full-bridge converter, which switch on and off to regulate the power flow through the transformer.

The third side of the circuit is the inverter, configured in an H-bridge arrangement. This stage converts the high-voltage DC (400V) to AC. The H-bridge configuration allows for the DC to AC conversion, producing a sinusoidal waveform suitable for AC loads. An LC filter, comprising specific inductance and capacitance values, is utilized to smooth the output waveform. This ensures that the output signal is a clean sinusoidal AC waveform. The duty ratio (D) of 0.7 indicates that the inverter MOSFETs are on for 70% of the switching period, ensuring efficient conversion and control of the output waveform. The filter values for the DC-DC and DC-AC stages are carefully selected to achieve this smoothing effect.

The design parameters and performance metrics for the dual-stage full-bridge microinverter, as shown in Table 3-4, include an input voltage (Vin) of 115V DC from the PV panel and an output voltage (Vout) of 246.07 Vrms AC, which is suitable for household or grid use. The table details the essential parameters such as output current (IL) of 2.051A, output power (Pout) of 504.6W, transformer ratio of 1:4, duty ratio (D) of 0.7, and specific values for filter inductance and capacitance in both DC-DC and DC-AC stages. Additionally, it outlines the load resistance (Rload) of 200 ohms and the series-parallel configuration of the PV panels, providing a comprehensive overview of the components and specifications used in the microinverter design.

Table 3-4 : Dual-Stage Full-Bridge Microinverter

Parameters	**Value**
Vin	115 V
Vout	246.07 Vrms
IL	2.051 A
Pout	504.6W
Transformer ratio	1:4
Duty Ratio, D	0.7
Filter Inductance, L (DC-DC)	50mH
Filter Capacitance, C (DC-DC)	1200μF
Filter Inductance, L (DC-AC)	30mH
Filter Capacitance, C (DC-AC)	30μF
Rload	200
Series	2
Parallel	1

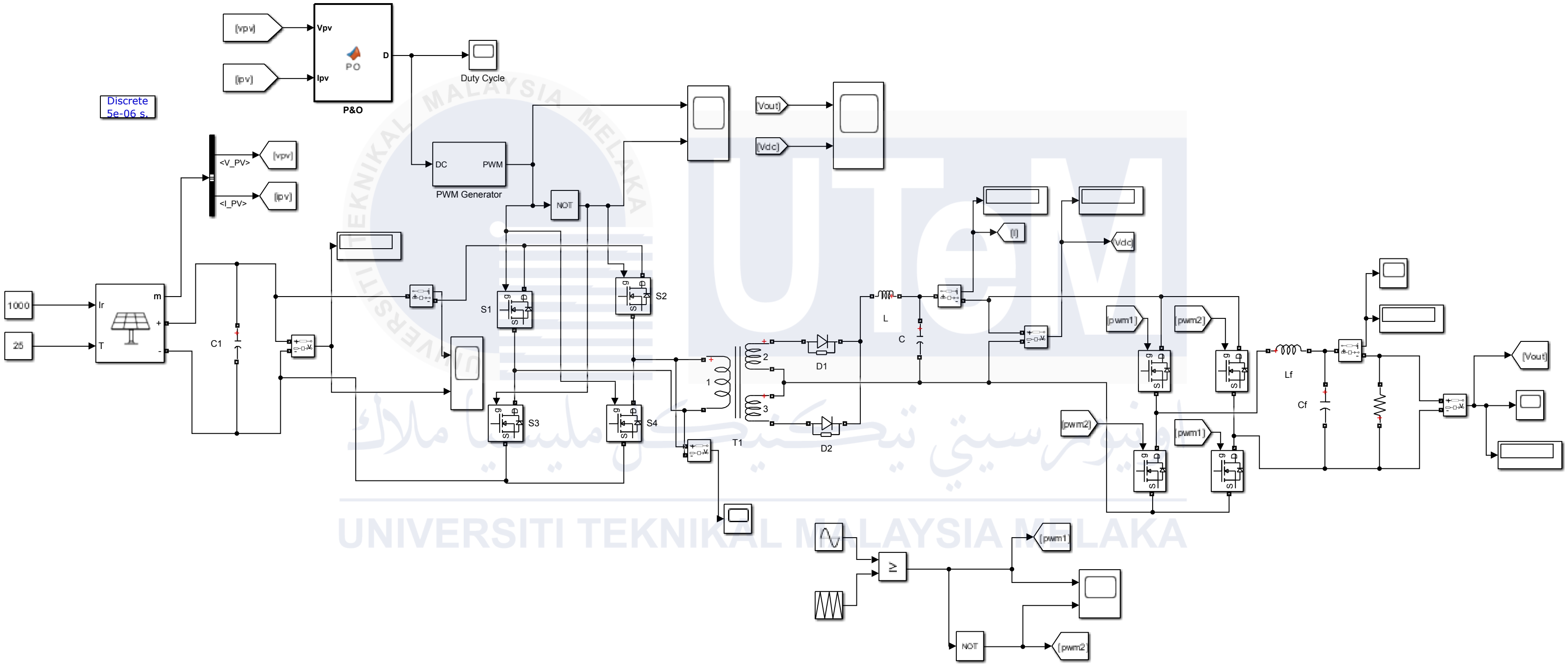

Figure 3-16 : Dual-stage Full-Bridge Microinverter

3.13 Limitation of proposed methodology

In this proposed methodology, only the full-bridge converter, H-bridge inverter, full-bridge PV microinverter, and dual-stage full-bridge microinverter are designed. All circuits are created and simulated using MATLAB/SIMULINK software, with no hardware implementation involved.

3.14 Summary

This chapter provides a comprehensive overview of the techniques and circuits designed for the project. It begins by outlining the methodology introduced at the start, including both the project flowchart and the circuit flowchart. The first design discussed is the full-bridge DC-DC converter, which is responsible for regulating DC voltage levels. This section includes detailed calculations for output voltage, current, and power, as well as the circuit design and simulation setup parameters. The chapter also covers the full-bridge PV microinverter, detailing its specific simulation setup and settings, and explaining the Perturb and Observe (P&O) algorithm method used. Additionally, the design and operation of the single-phase inverter are discussed. Furthermore, the dual-stage full-bridge PV microinverter is examined, including its design, simulation, and the methodology employed to achieve the desired performance metrics. All circuits are designed and simulated using MATLAB/SIMULINK software, with no hardware implementation, allowing for efficient optimization and validation of the designs through software simulations.

CHAPTER 4

RESULTS AND DISCUSSIONS

4.1 Introduction

This chapter provides the results obtained from the simulation experiments using MATLAB/Simulink. The focus is on the design and performance analysis of a full-bridge DC-DC converter and H-bridge inverter.

4.2 Simulation of Full-Bridge DC-DC Converter

As illustrated in Figure 4-1, it shows the simulation of the Full-bridge DC-DC converter in a open-loop system. The outcomes include a stable open-loop operation for full-bridge DC-DC converter aiming to achieve a 400V output.

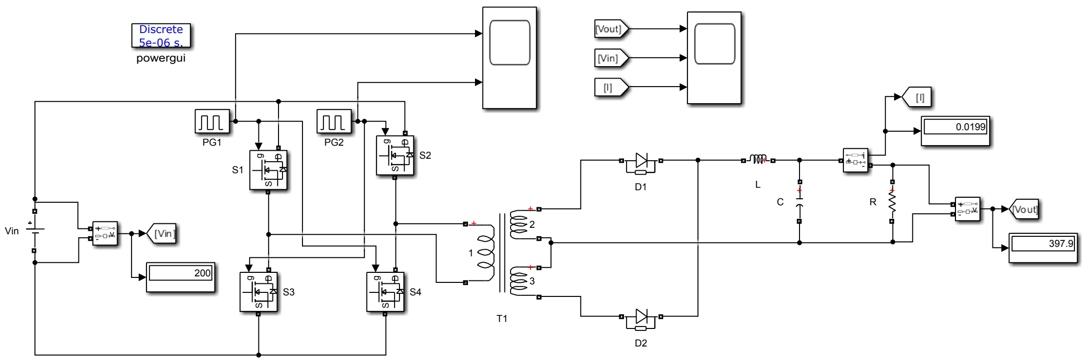

Figure 4-1: Simulation of the full-bridge DC-DC converter in an open-loop system

The output shown in Figure 4-2 appears to be in a DC state, as expected from the function of the DC-DC converter, which is designed to amplify the input voltage to a higher output voltage. In this specific design, the voltage amplification is achieved through a transformer with a turn's ratio of 1:2, meaning that the secondary winding has twice as many turns as the primary winding. This ratio directly influences the voltage increase, resulting in a significant boost from the input voltage. Through the simulation, an output voltage of 397.9V is obtained, demonstrating the converter's ability to effectively step up the voltage. Additionally, Figure 4-3 illustrates the input voltage waveform, which provides a detailed view of the initial voltage conditions before amplification. The smooth DC output indicates the successful transformation and regulation of the input voltage, maintaining a stable output suitable for the intended applications. This amplification process is crucial for applications requiring higher voltage levels, ensuring efficient power transfer and utilization.

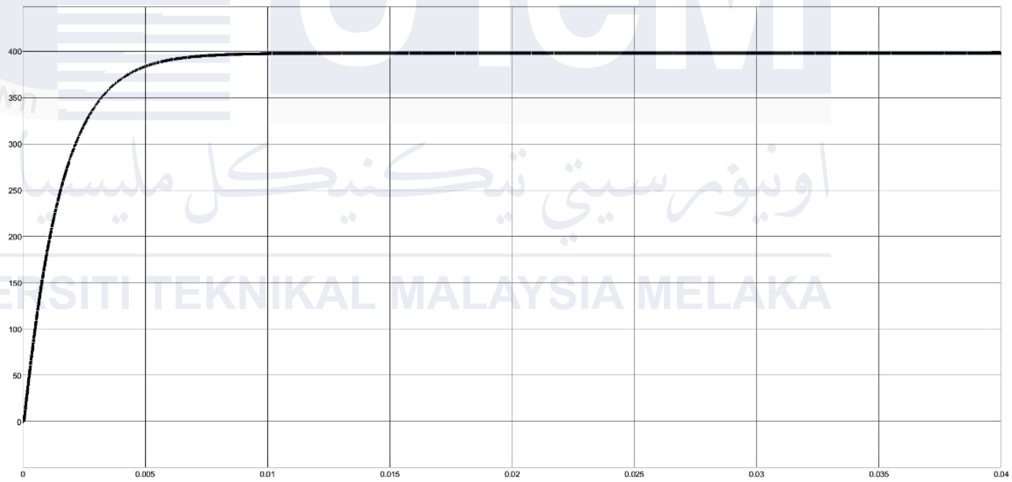

Figure 4-2: Voltage output for DC-DC converter circuit

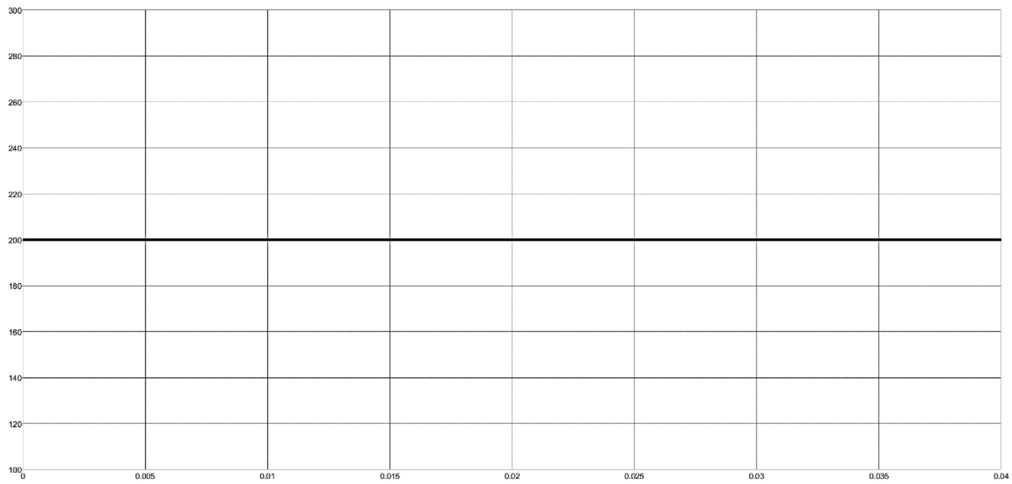

Figure 4-3: Voltage input for DC-DC converter circuit

Figure 4-3 illustrates the switching operation of the full-bridge converter, highlighting the coordinated control of the four MOSFETs (S1, S2, S3 and S4) to convert DC to AC. In this configuration, the MOSFETs are arranged in pairs, with S1 and S4 forming one diagonal pair and S2 and S3 forming the other. During operation, these MOSFETs switch on and off alternately to create a bidirectional current flow through the load. When S1 and S4 are turned on, the current flows in one direction, while switching S2 and S3 on creates a current flow in the opposite direction. The timing of these switches is controlled by pulse-width modulation (PWM) signals, which ensure that each pair is never on simultaneously, thus preventing short circuits.

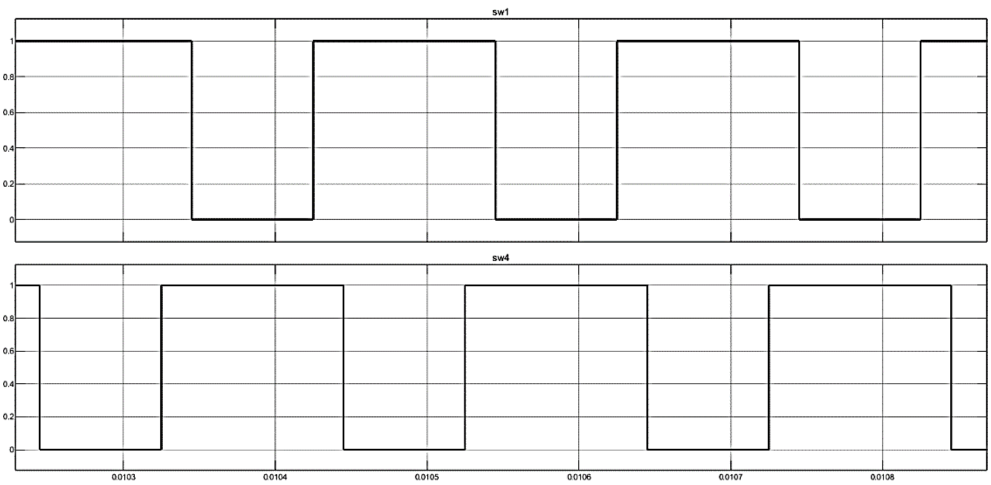

Figure 4-4: Switching of full-bridge converter

4.3 Analysis for Full-Bridge Converter

Table 4-1 presents a comparison between the calculated and simulated results, with the input voltage (Vin) kept constant throughout.

Table 4-1 : Comparison between Calculation and Simulation

Parameter	Calculation	Simulation
Vin	200V	200V
Vout	400V	399.1
Iout	1.25A	1.247A

In a full-bridge DC-DC converter, the output voltage is influenced by the duty ratio, which is the fraction of the switching cycle during which the primary side MOSFETs are conducting. The duty ratio determines how long the input voltage is applied to the transformer within each cycle, thereby affecting the voltage transferred to the secondary side. A higher duty ratio results in a longer conduction time, leading to an increase in the output voltage, while a lower duty ratio shortens the conduction time and decreases the output voltage. Table 4-2 demonstrates the impact of varying the duty cycle (D) on the output voltage (Vout) of a full-bridge converter.

Table 4-2 : Effect of duty ratio to output voltage

Duty Ratio, D	Output Voltage, Vout
0.4	385.4
0.5	389.2
0.6	393.1
0.7	399.5
0.8	408
0.9	419.3

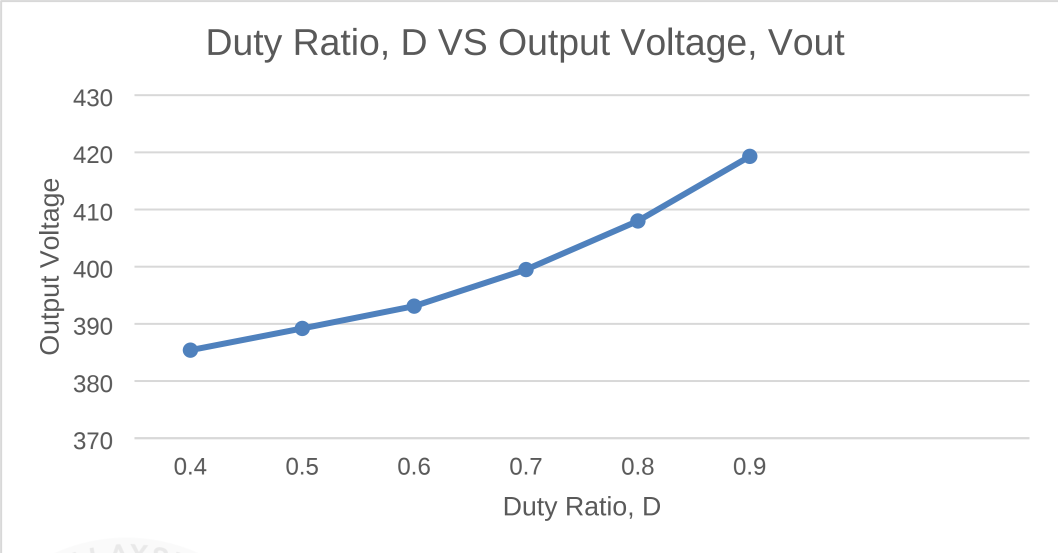

Figure 4-5: Voltage Output vs Duty Ratio

Based on the figure 4-5, it shows the graph of the output voltage against the duty cycle. The graph illustrates the effect of increment in duty cycle to the output voltage. The data compares output voltages for duty cycle values ranging from 0.4 to 0.9. As the duty cycle increases, the output voltage also increases. Specifically, the output voltage starts at 385.4V for a duty cycle of 0.4 and progressively rises to 419.3V at a duty cycle of 0.9. This shows a clear positive relationship between the duty cycle and the output voltage, indicating that higher duty cycles result in higher output voltages for the full-bridge converter.

4.4 Simulation of H-bridge Inverter

The simulations conducted for H-bridge inverter are expected to provide valuable insights into the system's performance. The outcomes include a stable open-loop operation for inverter aiming to achieve value of a 230V RMS output. Further analysis will assess the efficiency of the Maximum Power Point Tracking (MPPT) control system, evaluating its ability to optimize power extraction under varying operating conditions. These expected results will serve as a preliminary value for a comprehensive discussion on the effectiveness of the designed system in achieving the specified objectives.

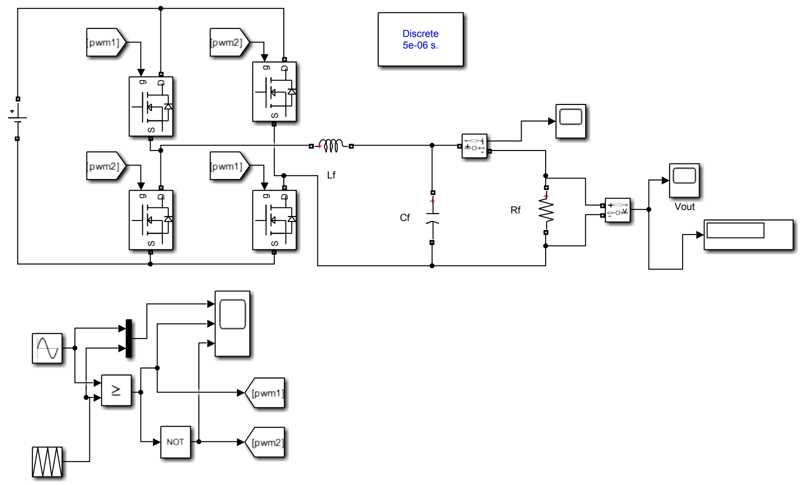

Figure 4-6: Simulation of H-bridge Inverter in an open-loop system

The H-bridge inverter simulation is study to examine the effect of different modulation indices on the output voltage. As illustrates in Figure 4-7, the waveform of simulation of an AC output voltage to achieved of 230Vrms. An LC filter with parameters 10µF and 5mH is utilized to smooth the output waveform. Figure 4-8 illustrates the corresponding output current waveform for the H-bridge inverter, which produces an output current of 2.26A. This setup highlights the effective regulation of voltage and current, demonstrating the inverter's capability to provide stable and reliable power output.

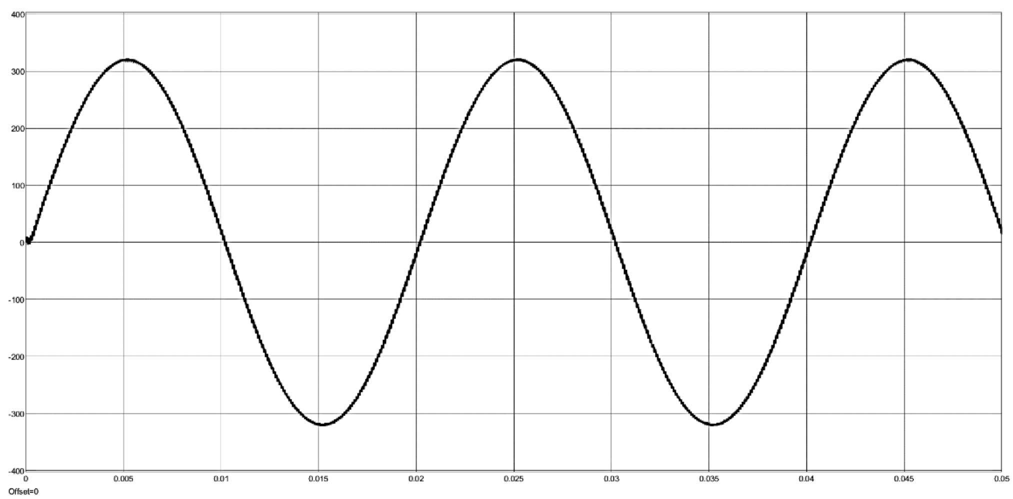

Figure 4-7: Output waveform of AC Voltage

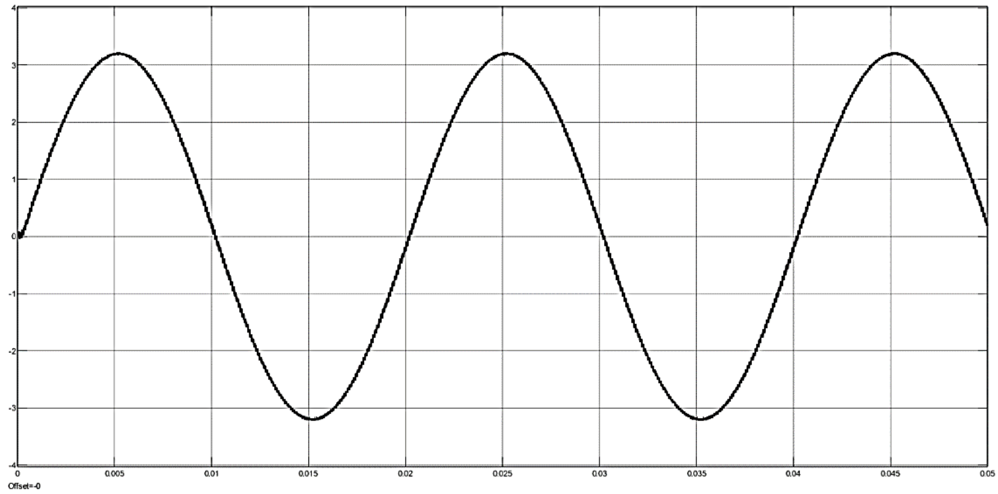

Figure 4-8: Output Current

Table 4-3 presents the impact of varying the modulation index on the output voltage of the H-bridge inverter. Throughout the experiments, the input voltage is consistently maintained at 400V DC, and the switching frequency is fixed at 20kHz. The output voltage is recorded in its peak form to accurately reflect the changes induced by different modulation indices. This setup ensures that the only variable influencing the output voltage is the modulation index, allowing for a clear analysis of its effect on the inverter's performance.

Table 4-3: H-bridge inverter analysis

Modulation amplitude, Ma	**Output Voltage, Vrms**
0.5	154
0.6	164.5
0.7	212
0.8	225.3
0.9	270.4

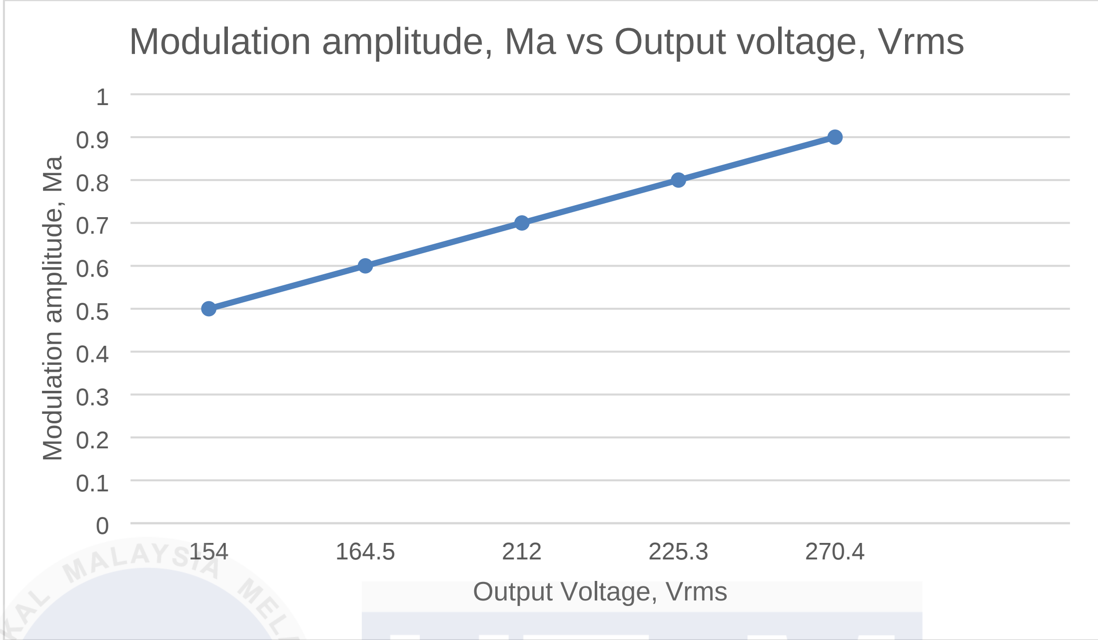

Figure 4-9: Output voltage vs Modulation index

4.5 Simulation of Full-Bridge dual-stage Microinverter

The first results obtained show the voltage output after the DC-DC converter, as illustrated in Figure 4-10. This figure depicts the Vdc at the converter side before converting the signal into AC voltage using the H-bridge inverter, and the waveform obtained should match the converter results shown in the figure. On the converter side, the transformer is set with a 1:4 ratio, producing the desired output at the converter side.

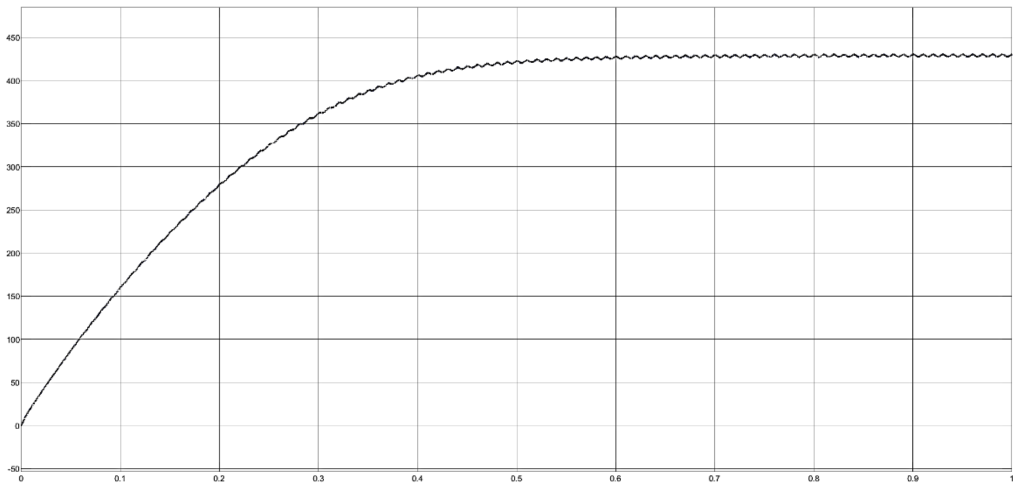

Figure 4-10 : Output Voltage produce at converter

Then, the output from the converter, with the addition of the LF filter, will produce a sinusoidal waveform at the inverter side, resulting in 230Vrms. The LF filter consists of an inductor with a value of 80 mH and a capacitor with a value of 20 μF. The load resistor (R load) is set to 120 ohms.

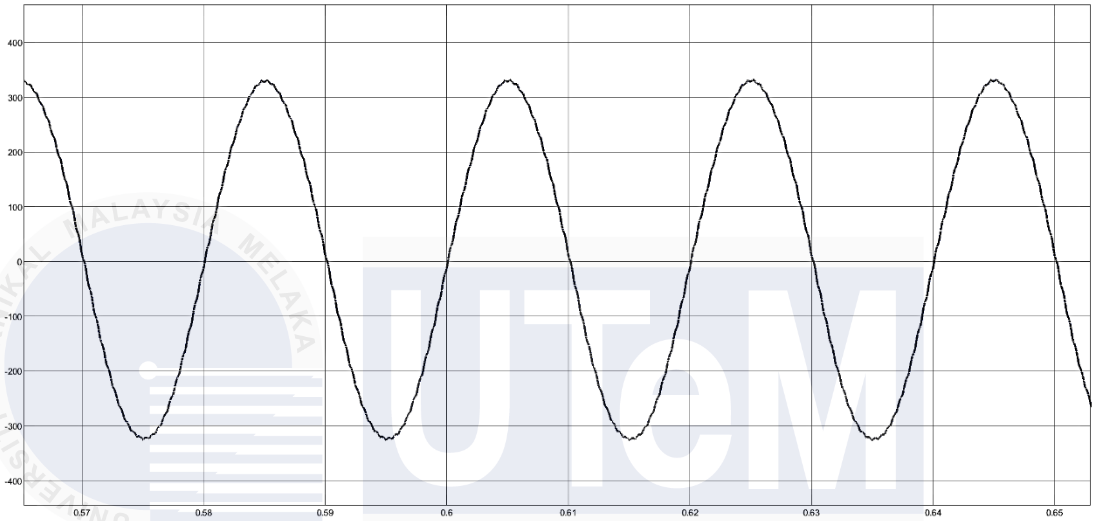

Figure 4-11: Output voltage produce at inverter

4.5.1 Analysis on R load

The analysis of the R load was conducted to assess the impact of various loads on THD (Total Harmonic Distortion). Specifically, the load parameter was set at 200**Ω**, and a modulation amplitude of 0.8 was applied. The LC filter was configured with values of 30 mH and 30 μF, combined with a 2 kHz repeating sequence block, to smooth out the waveform and provide a more stable voltage output. As a result of these settings, an AC voltage of 347V peak was achieved as shown in Figure 4-12

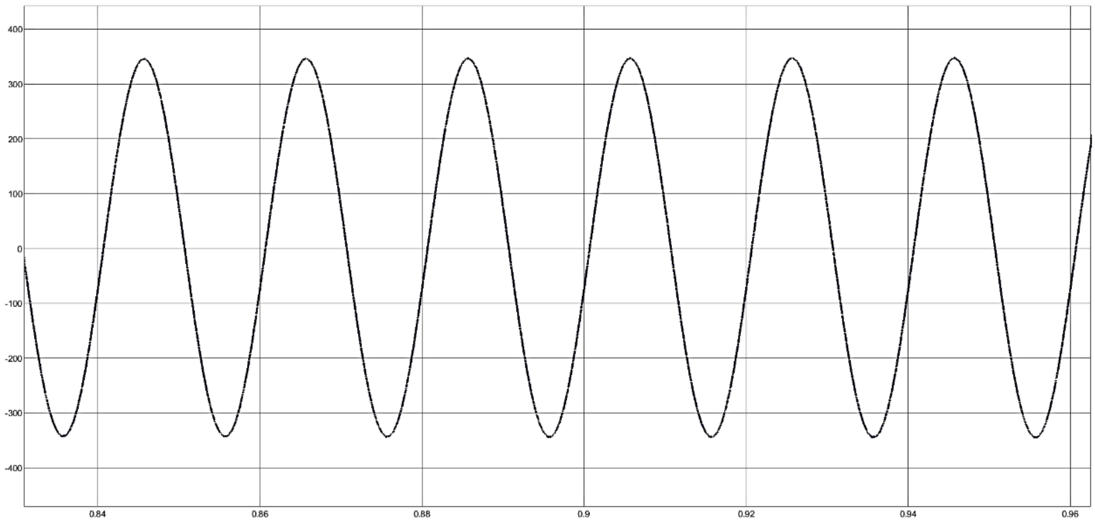

Figure 4-12 : Output AC Voltage on R load

Based on Figure 4-13, the output current waveform is illustrated. Both the output voltage and output current waveforms are expected to be sinusoidal. This simulation results in an output current of 2.9A. These results can provide the output power for the system. Based on the results, the product of output voltage in rms and output current in rms can achieve an output power of 504.7W.

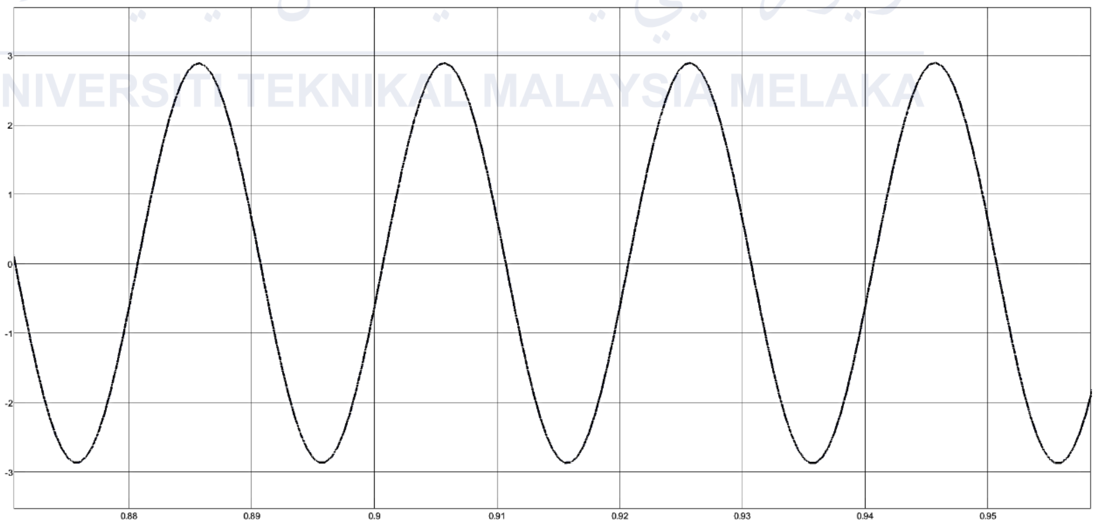

Figure 4-13 : Output current on R load

Figure 4-14 and Figure 4-15 illustrate the FFT analysis for the output voltage and output current, respectively. The harmonics at 2 kHz represent the harmonics at the switching frequency. The Total Harmonic Distortion (THD) is lower than 5%, indicating that the results are acceptable.

It is crucial to keep the THD below 5% because high levels of harmonic distortion can lead to performance issues with electrical components. Harmonics are highly sensitive to non-linear loads, such as computers and variable speed drives. Excessive THD can cause equipment breakdowns, overheating, increased wear and tear, decreased efficiency, and a shorter lifespan for the components. Therefore, maintaining a low THD is essential to ensure the reliability, efficiency, and longevity of electrical systems and devices.

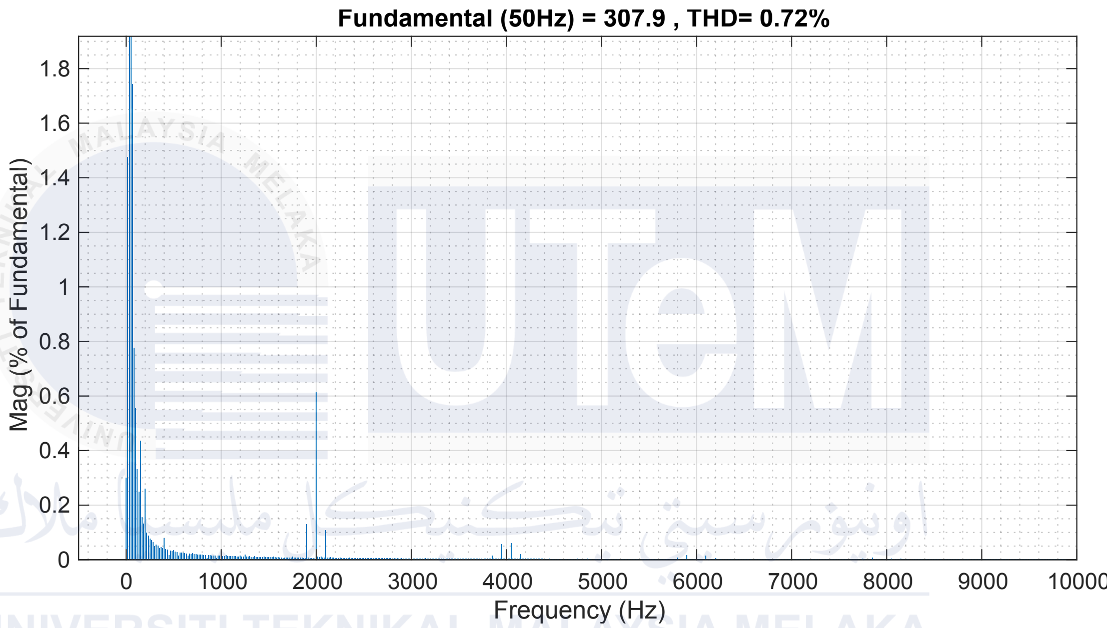

Figure 4-14 : FFT analysis on output voltage

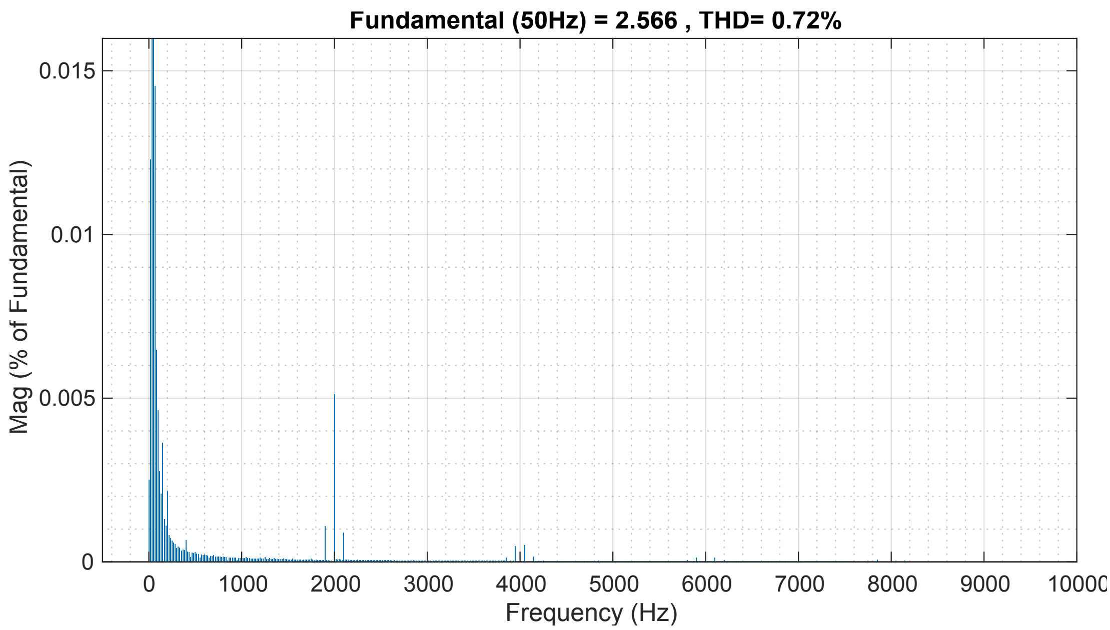

Figure 4-15 : FFT analysis on output current

4.5.2 Analysis on RL load

The analysis of the RL load was conducted to assess the impact of various loads on THD (Total Harmonic Distortion). Specifically, the RL load parameter was set at 100Ω and 100mH, and a modulation amplitude of 0.8 was applied. The LC filter was configured with values of 60mH and 50µF. As a result of these settings, an AC voltage of 327V peak was achieved. Figure 4-16 illustrate the output AC voltage for RL load.

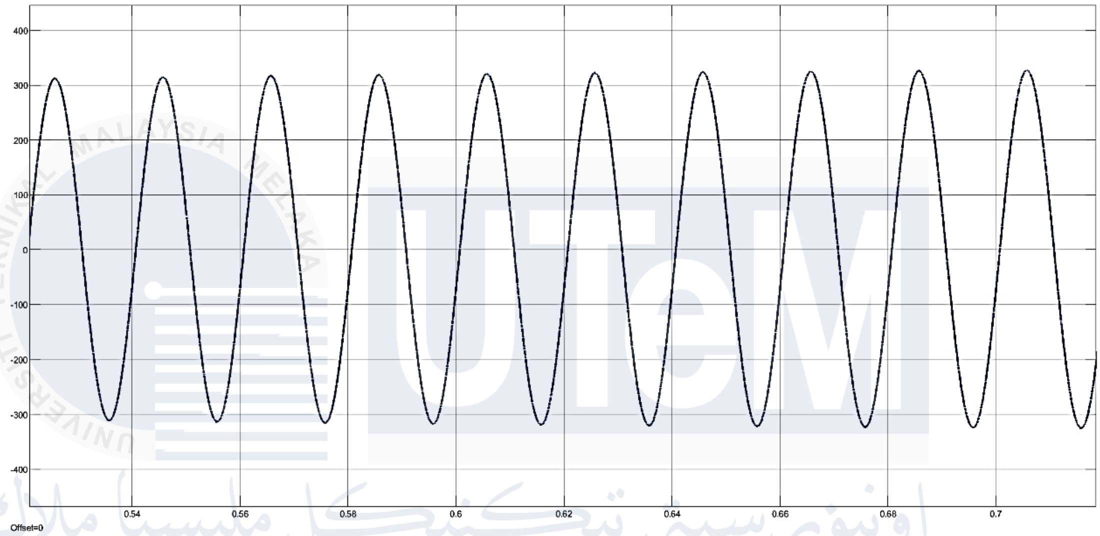

Figure 4-16 : Output AC Voltage on RL load

Based on Figure 4-17, the output current waveform is illustrated. Both the output voltage and output current waveforms are expected to be sinusoidal. This simulation results in an output current of 2.95A. These results can provide the output power for the system. Based on the results, the product of output voltage in rms and output current in rms can achieve an output power of 484.4W.

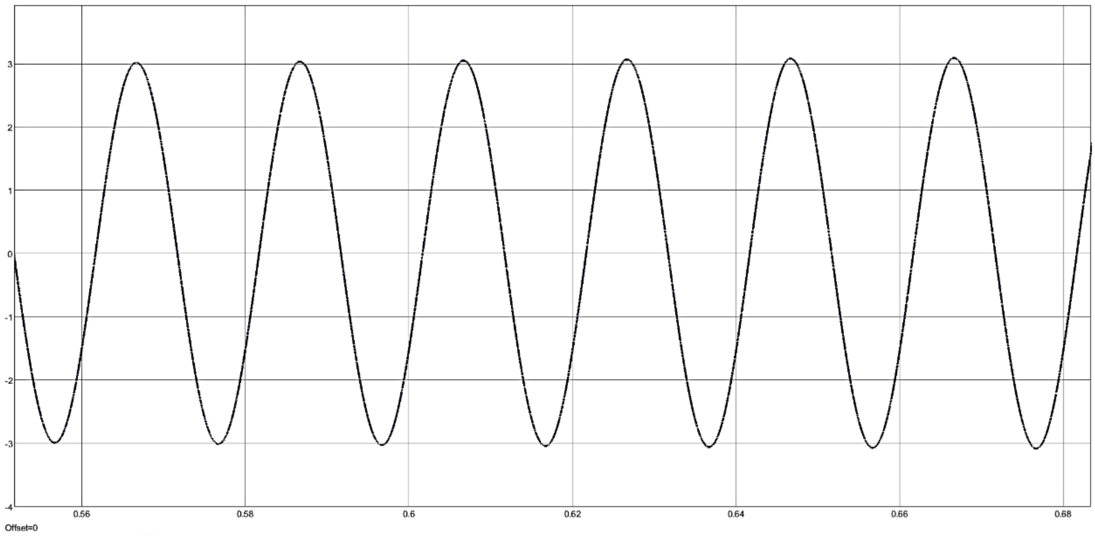

Figure 4-17: Output AC Current on RL load

Figure 4-18 shows the FFT analysis of the output voltage with an RL load, where the THD is 0.60%. Figure 4-19 shows the FFT analysis of the output current with an RL load, where the THD is 0.62%. Both values are below the 5% threshold.

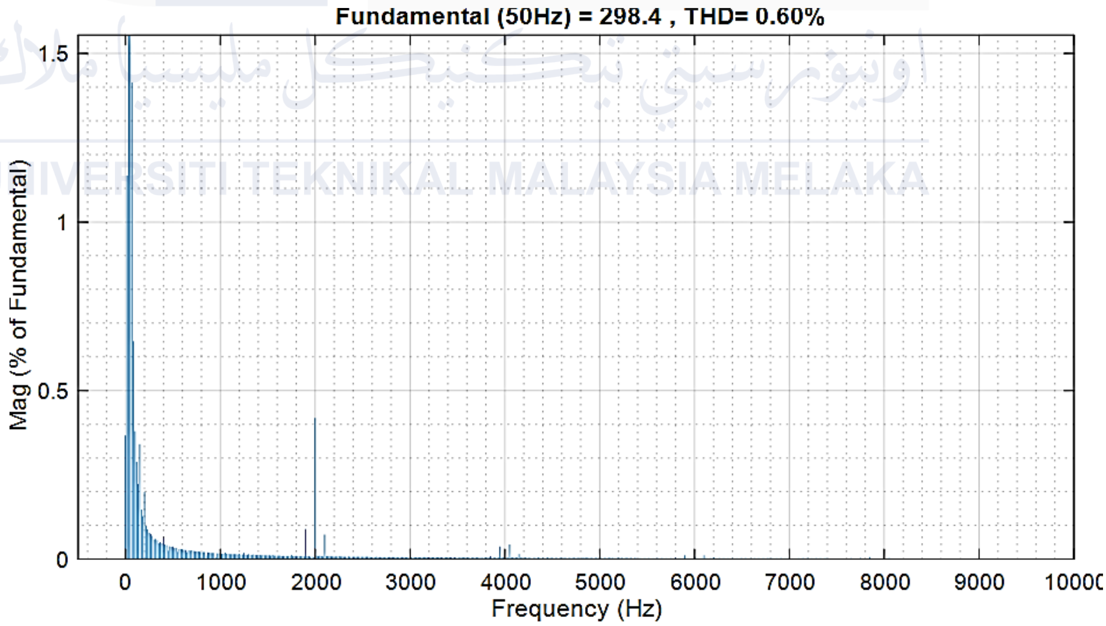

Figure 4-18: FFT analysis on output voltage with RL load

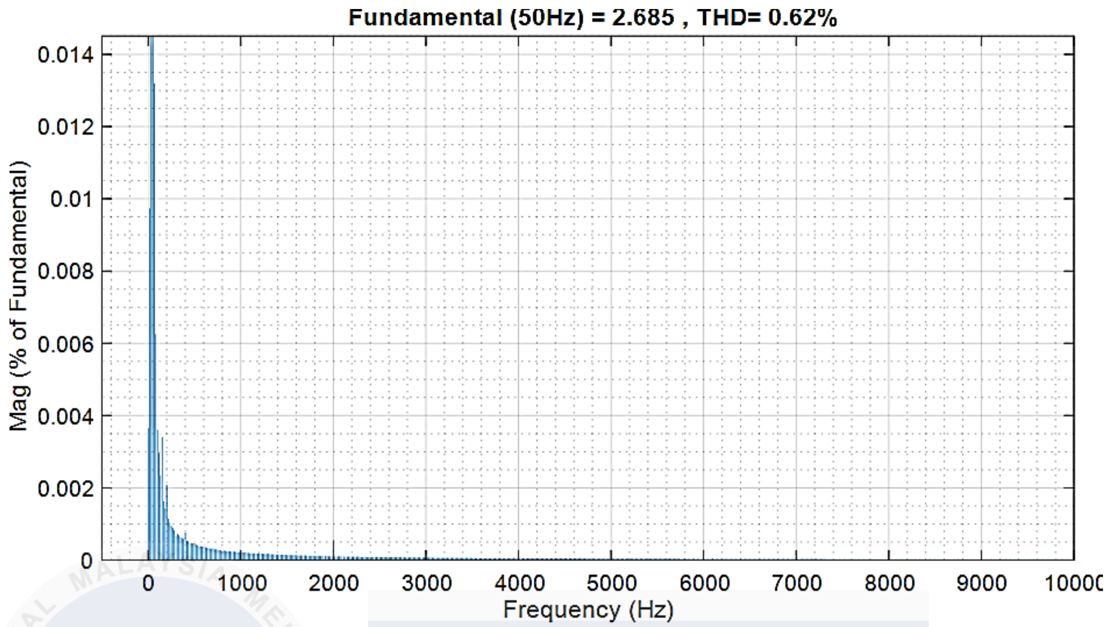

Figure 4-19 : FFT analysis on output current with RL load

4.6 THD comparison on dual-stage Full-Bridge PV microinverter

Table 4-4 illustrates the comparison on the THD analysis between two different types of load for the dual-stage full-bridge PV microinverter.

Table 4-4 :THD analysis for different load

Parameter	R load	RL load
AC output voltage	0.72%	0.62%
AC output current	0.72%	0.6%

Based on the data in Table 4-5, the effect of varying modulation amplitude on Irms and Vrms for R load can be observed.

Table 4-5 : Effect of varying Ma to Irms and Vrms for R Load

Modulation Amplitude, ma	Irms, A	THDi, %	Vrms, V	THDv, %
0.4	1.441	0.78	173.24	0.78
0.5	1.754	1.09	210.72	1.09
0.6	1.973	1.04	236.88	1.04
0.7	2.051	0.72	246.07	0.72
0.8	1.980	1.00	237.59	1.00
0.9	1.867	1.06	224.15	1.06

Figure 4-20 illustrates the relationship between the modulation amplitude (Ma) and the root mean square current (Irms) for an R load. As the modulation amplitude increases from 0.4 to 0.9, Irms initially rises, reaching a peak at Ma = 0.7, after which it begins to decline slightly. This behavior indicates the response of the current to varying levels of modulation amplitude in a resistive load.

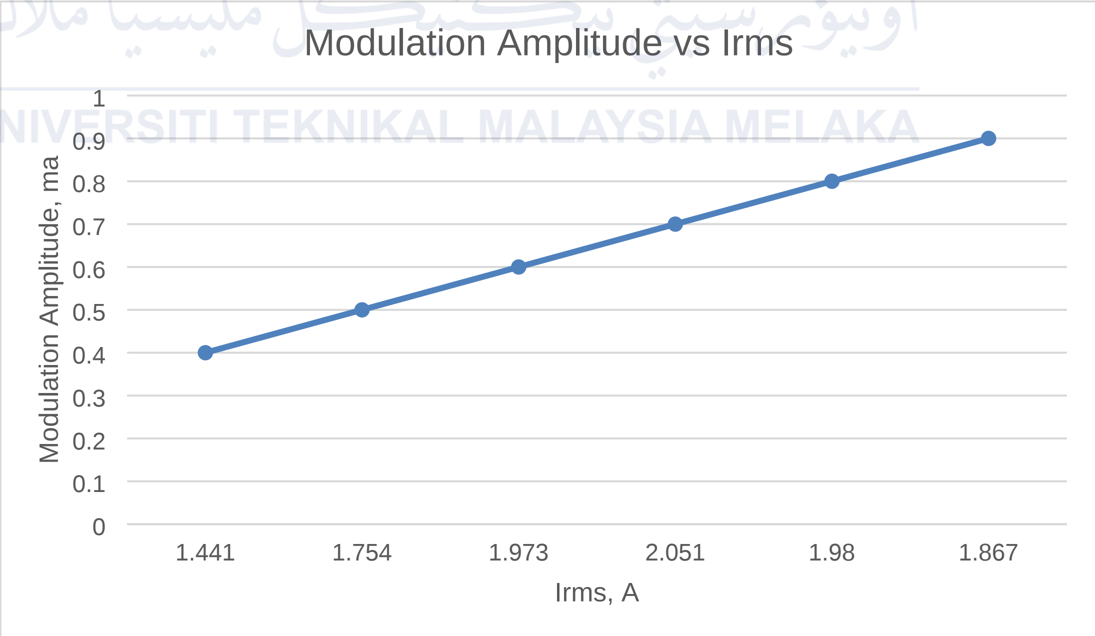

Figure 4-20 : Modulation amplitude, Ma vs Irms, A for R load

Figure 4-21 shows the relationship between the modulation amplitude (Ma) and the root mean square voltage (Vrms) for an R load. The Vrms increases almost linearly with the increase in modulation amplitude, peaking at Ma = 0.7 before slightly decreasing. This trend demonstrates how the output voltage varies with changes in modulation amplitude for a resistive load.

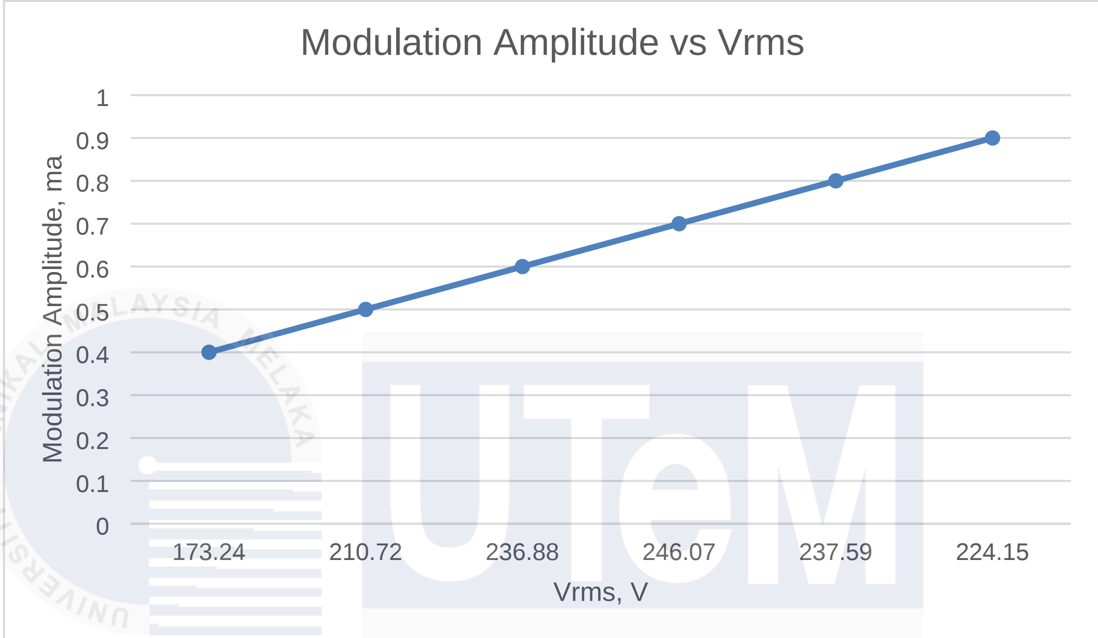

Figure 4-21 : Modulation amplitude, ma vs Vrms, V for R load

Figure 4-22 depicts the total harmonic distortion of current (THDi) versus the root mean square current (Irms) for an R load. The graph indicates that THDi generally fluctuates with changes in Irms, showing peaks and troughs that suggest non-linear relationships between the harmonic distortion and current magnitude. The lowest THDi is observed at Ma = 0.7, which corresponds to the peak Irms.

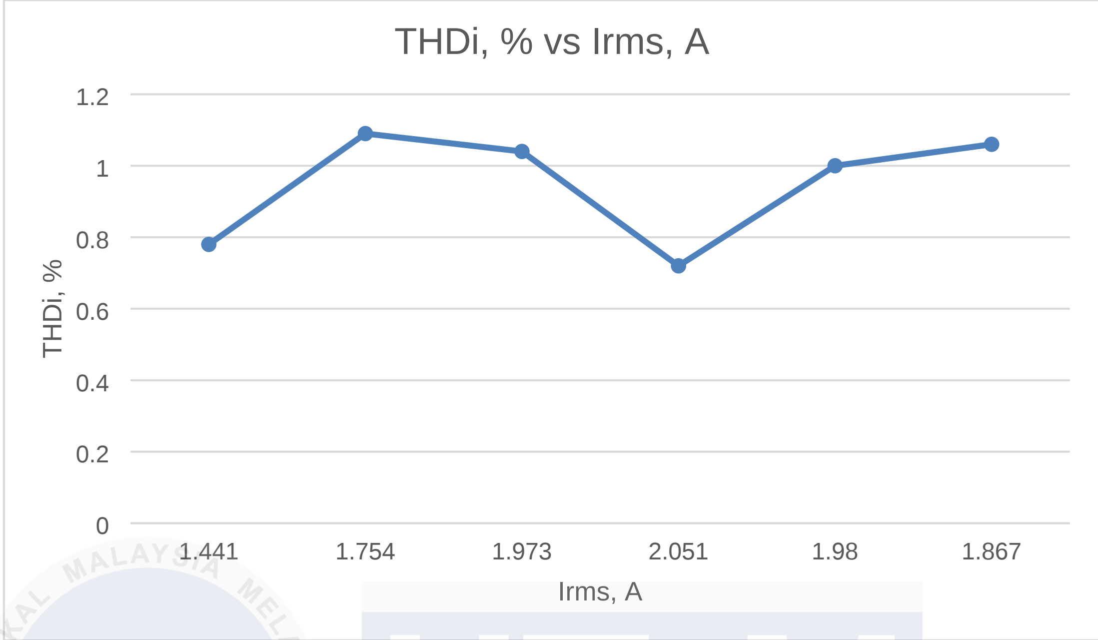

Figure 4-22 : THDi, % vs Irms, A for R load

Figure 4-23 presents the total harmonic distortion of voltage (THDv) versus the root mean square voltage (Vrms) for an R load. The THDv shows a pattern similar to THDi, with the lowest distortion occurring at Ma = 0.7, corresponding to the highest Vrms value. This indicates that both current and voltage harmonic distortions are minimized at this modulation amplitude.

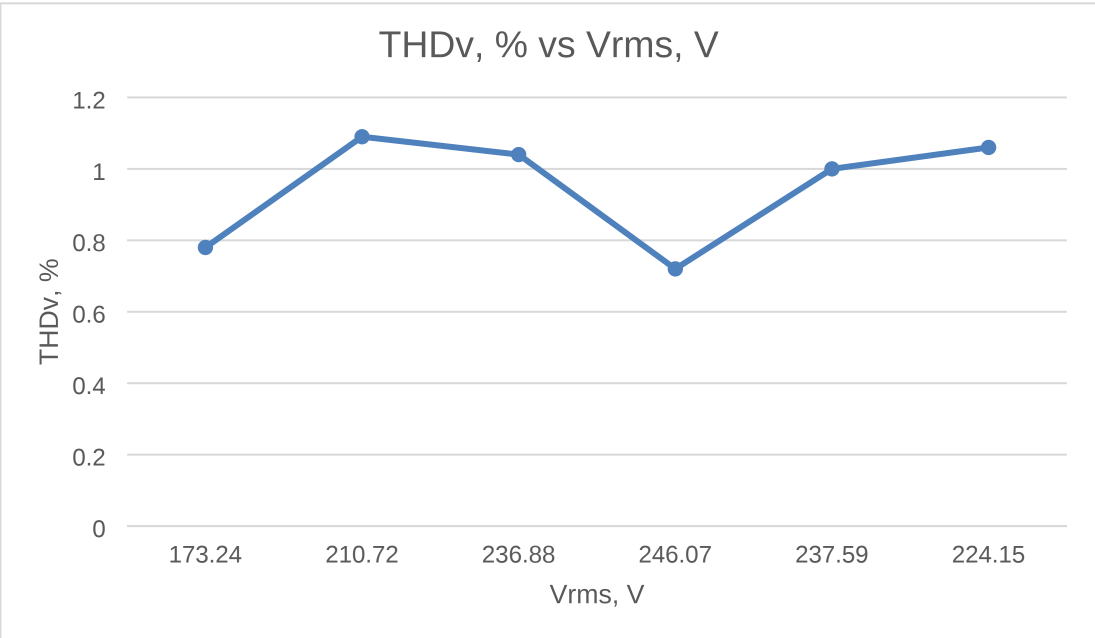

Figure 4-23 : THDv, % vs Vrms, V for Rload

Table 4-6 : Effect of varying Ma to Irms and Vrms for RL Load

Modulation Amplitude, Ma	Irms	THDi	Vrms	THDv
0.4	1.631	0.72	181.44	0.75
0.5	1.965	1.00	218.85	0.97
0.6	2.121	0.88	236.46	0.87
0.7	2.09	0.62	231.72	0.6
0.8	1.965	0.63	219.7	0.64
0.9	1.845	0.59	205.34	0.61

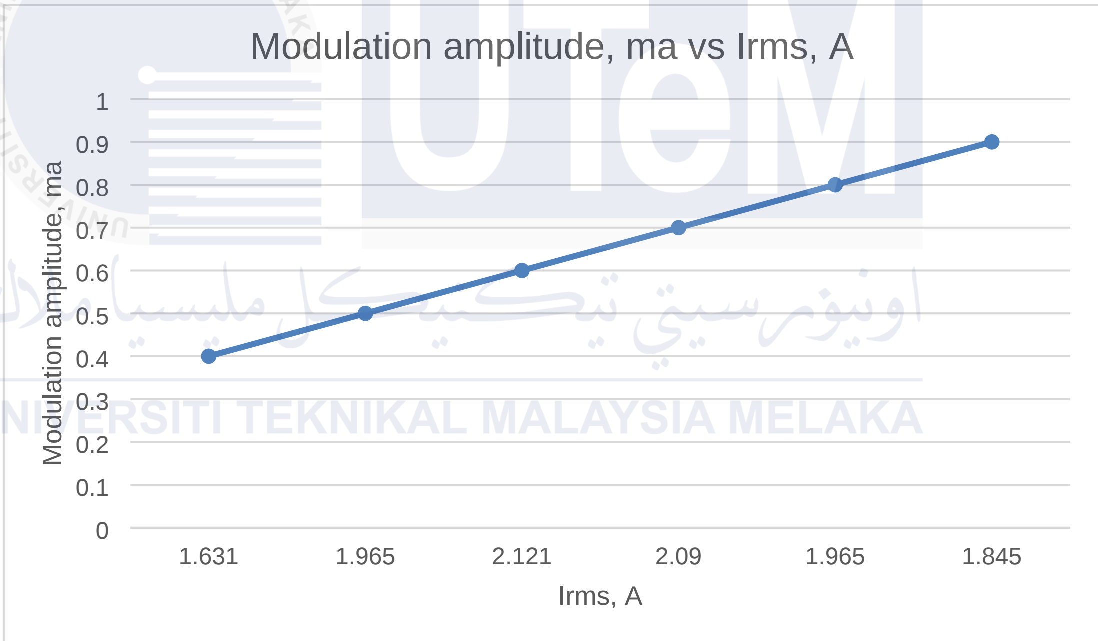

Figure 4-24: Modulation amplitude, ma vs Irms,A for RL load

Figure 4-24 illustrates the relationship between the modulation amplitude (Ma) and the root mean square current (Irms) for an RL load. As the modulation amplitude increases from 0.4 to 0.9, Irms increases steadily, reaching a peak at Ma = 0.6, after which it decreases slightly. This pattern indicates how the current responds to varying modulation amplitudes in a resistive-inductive load.

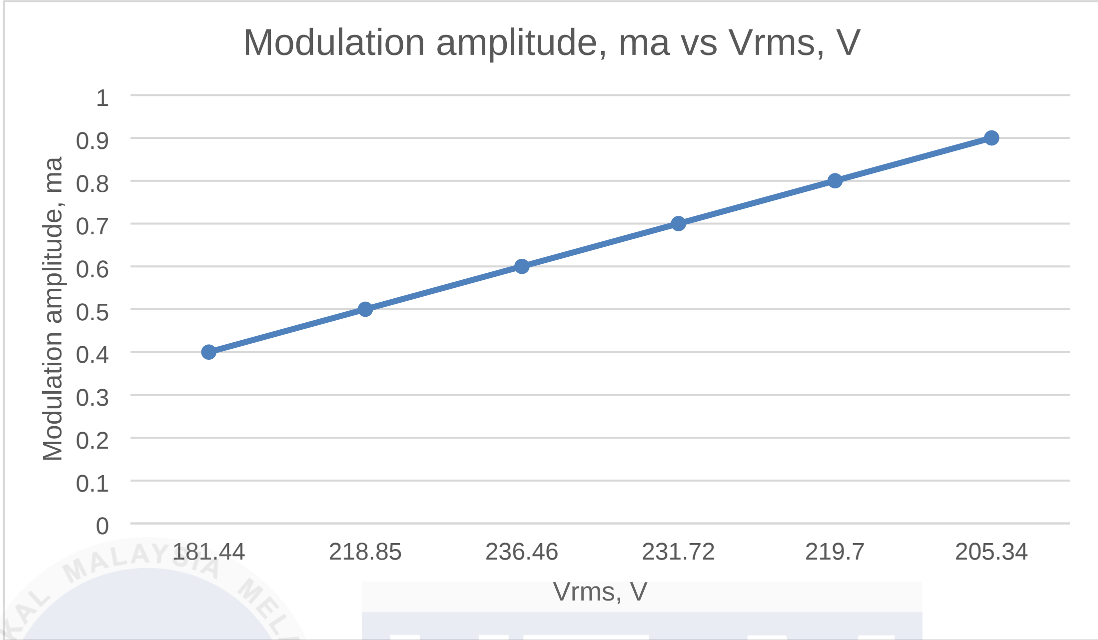

Figure 4-25: Modulation amplitude, ma vs Vrms,V for RL load

Figure 4-25 shows the relationship between the modulation amplitude (Ma) and the root mean square voltage (Vrms) for an RL load. The Vrms increases with the modulation amplitude, peaking at Ma = 0.6 before experiencing a slight decline. This trend demonstrates the variation in output voltage with changes in modulation amplitude for a resistive-inductive load.

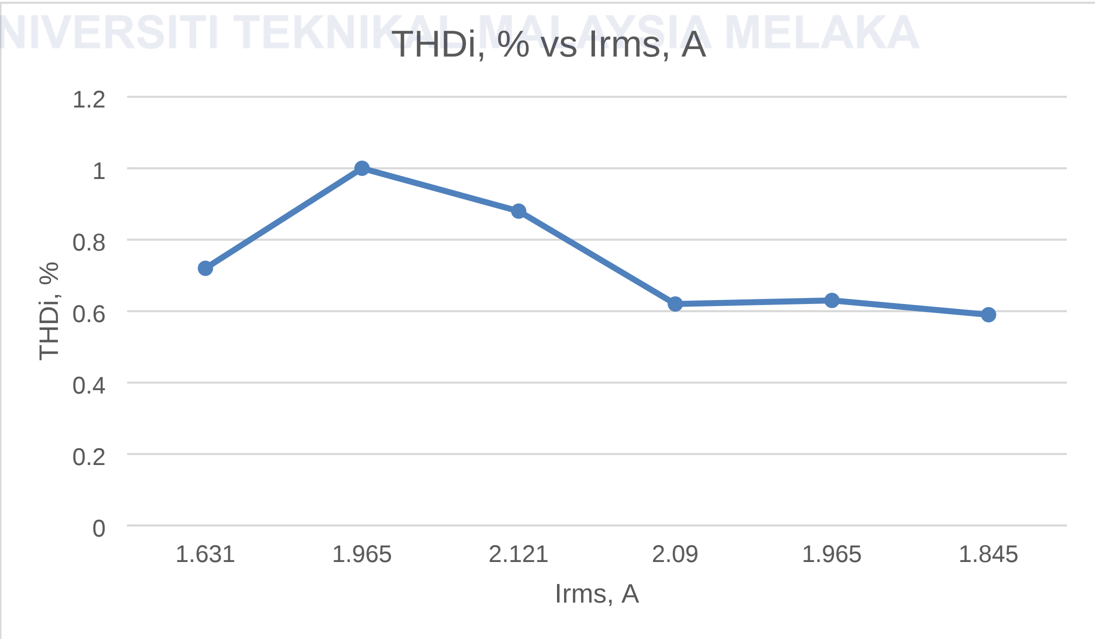

Figure 4-26 : THDi, % vs Irms, A for RL load

Figure 4-26 depicts the total harmonic distortion of current (THDi) versus the root mean square current (Irms) for an RL load. The graph shows that THDi generally decreases as Irms increases, reaching the lowest distortion at Ma = 0.9. This indicates a more linear relationship between harmonic distortion and current in a resistive-inductive load compared to a purely resistive load.

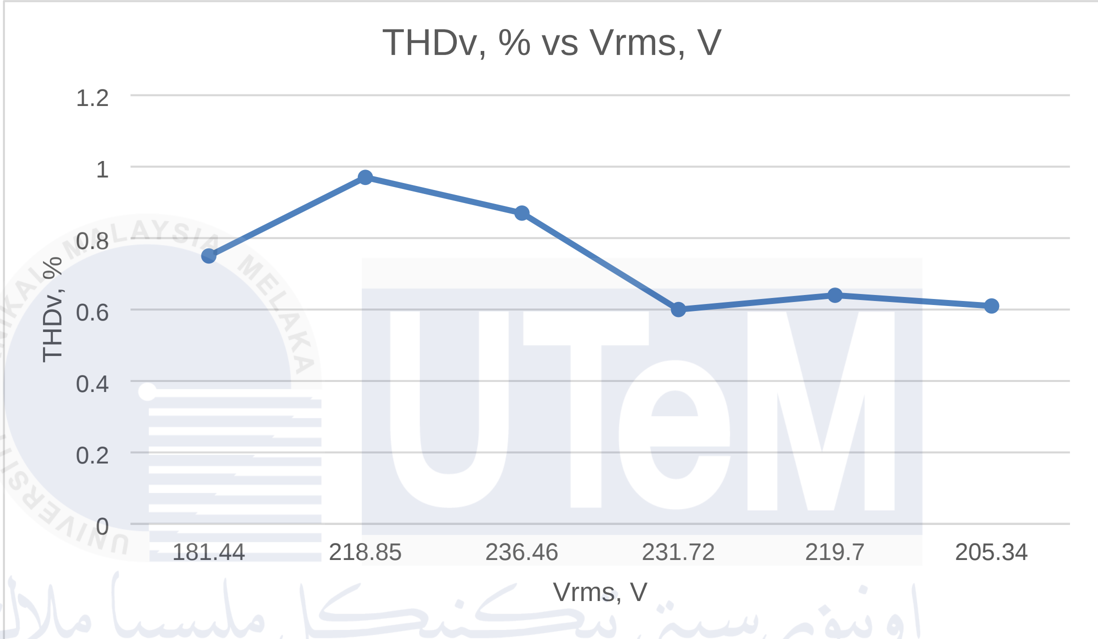

Figure 4-27 : THDv, % vs Vrms, V for RL load

Figure 4-27 presents the total harmonic distortion of voltage (THDv) versus the root mean square voltage (Vrms) for an RL load. Similar to the current distortion, THDv decreases as Vrms increases, with the lowest distortion observed at Ma = 0.9. This trend suggests that both current and voltage harmonic distortions are minimized at higher modulation amplitudes in a resistive-inductive load.

Table 4-7 illustrates the output power comparison for different type of loads for the system of dual-stage full-bridge PV microinverter.

Table 4-7 :Comparison of Output power for R load and RL load

Parameter	**R load**	**RL load**
Input power	550W	550W
Output power	504.7W	484.3W

Based on the data in Table 4-5, the efficiency of the dual-stage full-bridge PV microinverter can be obtained. The efficiency of the microinverter for each load type can be calculated using the formula (4.1)

$$\text{Efficiency},\eta\ (\%) = \left(\frac{\text{Output power}}{\text{Input power}}\right)\text{x}100 \tag{4.1}$$

For the R load

$$\text{Efficiency},\eta\ (\%) = \left(\frac{504.7}{550}\right)\text{x}100 = 91.76\%$$

For the R load

$$\text{Efficiency},\eta\ (\%) = \left(\frac{484.3}{550}\right)\text{x}100 = 88.05\%$$

The calculated efficiencies show that the microinverter achieves approximately 91.76% efficiency with an R load, while its efficiency drops slightly to around 88.05% with an RL load. This decrease is due to the inductive component in the RL load, which causes additional losses such as reactive power losses and potentially higher switching losses in the inverter.

4.7 Summary

Thorough simulation of the full-bridge converter circuit's connected systems, integration with a photovoltaic (PV) system, and the integrated configuration with an inverter are all included in this chapter. Performance parameters including voltage stability, current efficiency, power output, modulation amplitude impacts, and load responses were carefully evaluated at each phase. At first, the independent full-bridge converter circuit showed dependable DC voltage conversion skills, guaranteeing consistent output characteristics necessary for a variety of uses. Efficiency in using solar energy was greatly improved by MPPT algorithm implementation and integration with the PV system. This stage demonstrated enhanced rates of power conversion and output optimization in a range of environmental circumstances. As a result of the integration with the inverter, consistent sinusoidal waveforms appropriate for AC loads were produced, enabling the comprehensive analysis included modulation amplitude variations and load type evaluations, revealing optimal settings to minimize Total Harmonic Distortion (THD) and maximize operational efficiency across different load scenarios.

CHAPTER 5

CONCLUSION AND RECOMMENDATIONS

5.1 Conclusion

In conclusion, this project addresses challenges in the efficiency of standalone photovoltaic systems, focusing on improving the maximum power point tracking (MPPT) algorithm for a full-bridge microinverter in small-scale and distributed applications. The identified issues, including power generation limitations due to atmospheric conditions and module failures, necessitate the development of a full-bridge DC-DC converter and an efficient MPPT controller. The project's scope involves MATLAB/Simulink simulations, encompassing the design of an H-bridge inverter, integration of a 500W power-rated full-bridge DC-DC converter, and a comparative analysis of the microinverter's efficiency with a string inverter. The overarching goal is to strike a balance between accuracy and simplicity while ensuring cost-effectiveness for optimal performance in small-scale photovoltaic systems.

5.2 Future Works

Having completed the design, simulation, and validation of the full-bridge converter integrated with a solar PV system and MPPT algorithm, the next steps can focus on several advanced topics. First, prioritize hardware implementation and testing by building a physical prototype to validate simulation results in real-world conditions. This includes sourcing components, assembling the circuit, and conducting tests to assess performance, efficiency, and stability, providing insights and revealing practical issues. Next, explore advanced control strategies such as adaptive control, fuzzy logic, or neural networks for MPPT to enhance efficiency and response time under changing conditions. Additionally, investigate integrating battery storage with the PV system to manage energy supply effectively, designing control mechanisms to optimize efficiency and lifespan.

Developing a grid-tied inverter system will allow the PV system to feed power back into the grid, requiring compliance with regulations and implementing synchronization techniques. Conduct long-term performance and reliability studies to understand system durability and economic viability over time. Finally, perform an economic and environmental analysis of the system, including cost-benefit assessments and potential carbon footprint reduction, to demonstrate the system's broader impact and sustainability. These future works aim to transition from simulation to practical implementation and explore advanced techniques to enhance overall system performance and sustainability.

REFERENCES

[1] Zakhidov RA. Central Asian countries energy system and role of renewable energy sources. Applied Solar Energy 2008;44(3):218–23

[2] Bergmann A, Colombo S, Hanley N. Rural versus urban preferences for renewable energy developments. Ecological Economics 2008; 65:616–25.

[3] IRENA (2018c), Renewable Power Generation Costs in 2017, International Renewable Energy Agency (IRENA), Abu Dhabi.

[4] Bie, Z., Lin, C., Li, G., &Qiu, A. (2020). Development and Prospect of Resilient Power System in the Context of Energy Transition. Journal of Chinese Society for Electrical Engineering, 40(9), 2735.

[5] L. Zhang, W. G. Hurley and W. Wolfle, "A New Approach to Achieve Maximum Power Point Tracking for PV System with a Variable Inductor," 2nd IEEE International Symposium on Power Electronics for Distributed Generation Systems, pp. 948-952, 2010

[6] Youm I, Sarr J, Sall M, Kane MM. Renewable energy activities in Senegal: a review. Renewable and Sustainable Energy Reviews 2000;4(1):75–89

[7] Rathore NS, Panwar NL. Renewable energy sources for sustainable development. New Delhi, India: New India Publishing Agency; 2007

[8] Zakhidov RA. Central Asian countries energy system and role of renewable energy sources. Applied Solar Energy 2008;44(3):218–23.

[9] Bhatti, Harrison. (2021). The future of sustainable society–The state of the art of renewable energy and distribution systems. 10.13140/RG.2.2.25281.28008/1.

[10] N. Khordehgah, V. Guichet, S.P. Lester, H. Jouhara, Computational study and experimental validation of a solar photovoltaics and thermal technology, Renew. Energy 143 (2019) 1348–1356

[11] A. Luque, S. Hegedus, "Handbook of Photovoltaic Science and Engineering", John Wiley & Sons Ltd, West Sussex, England, 2003.

[12] Gao, Lijun & Dougal, Roger & Liu, Shengyi & Iotova, Albena. (2009). Parallel-Connected Solar PV System to Address Partial and Rapidly

Fluctuating Shadow Conditions. Industrial Electronics, IEEE Transactions on. 56. 1548 - 1556. 10.1109/TIE.2008.2011296.

[13] Shimizu, Toshihisa & Hirakata, Masaki & Kamezawa, Tomoya & Watanabe, Hisao. (2001). Generation control circuit for photovoltaic modules. Power Electronics, IEEE

[14] T. Tafticht, K. Agbossou, M.L. Doumbia and A. Cheriti, “An improved maximum power point tracking method for photovoltaic system”, Renewable Energy, vol. 33, pp. 1508-1516, 2008

[15] Fathabadi, Hassan. (2016). Novel high accurate sensorless dual-axis solar tracking system controlled by maximum power point tracking unit of photovoltaic systems. Applied Energy. 173. 448-459. 10.1016/j.apenergy.2016.03.109.

[16] Tajuddin, Mohammad Faridun Naim & Md, Shahrin & Arif, M Saad & Salam, Zainal. (2015). Perturbative Methods for Maximum Power Point Tracking (MPPT) of Photovoltaic (PV) Systems: A Review. International Journal of Energy Research. 10.1002/er.3289

[17] Mazen Abdel-Salam, Mohamed-Tharwat El-Mohandes, Mohamed Goda, (2018) An improved perturb-and-observe based MPPT method for PV systems under varying irradiation levels

[18] Deng, Wenpeng & Amaratunga, Gehan. (2014). Limits of Incremental Conductance for determining the Maximum Power Point under rapidly changing irradiance and an alternative technique based on fast scanning. 2014 IEEE 40th Photovoltaic Specialist Conference, PVSC 2014. 3690-3694. 10.1109/PVSC.2014.6924908

[19] J Ahmed, Z Salam, A Maximum Power Point Tracking (MPPT) for PV system with partial shading capability, Applied Energy 119 (2014), 118-130

[20] Palanisamy R, Vijayakumar K, Venkatachalam V, et al. Simulation of various DC-DC converters for photovoltaic system. International Journal of Electrical and Computer Engineering (IJECE), 2019, 9:917.

[21] Xi, Y.; Jain, P.K. A forward converter topology with independently and precisely regulated multiple outputs. IEEE Trans. Power Electron. 2003, 18, 648–658

[22] Abramovitz, A.; Cheng, T.; Smedley, K. Analysis and Design of Forward Converter With Energy Regenerative Snubber. IEEE Trans. Power Electron. 2010, 25, 667–676

[23] Alhurayyis, I.; Elkhateb, A.; Morrow, J. Isolated and nonisolated DC-to-DC converters for medium-voltage DC networks: A review. IEEE J. Emerg. Sel. Top. Power Electron. 2020, 9, 7486–7500

[24] Whitaker, B.; Martin, D.; Cilio, E. Extending the operational limits of the push-pull converter with SiC devices and an active energy recovery clamp circuit. In Proceedings of the 2015 IEEE Applied Power Electronics Conference and Exposition (APEC), Charlotte, NC, USA, 15–19 March 2015; pp. 2033–2038

[25] Bilsalam, A.; Ekkaravarodome, C.; Chunkag, V.; Thounthong, P. Analyzing the Effect of Parasitic Capacitance in a Full-Bridge Class-D Current Source Rectifier on a High Step-Up Push–Pull Multiresonant Converter. Sustainability 2021, 13, 5477

[26] Abd Rahim, Nasrudin & Mohamad Elias, Mohamad Fathi & Jamaludin, Jafferi & Rivai, Ahmad & Erixno, Oon & Zainal, Febry Yadi. (2016). Design and implementation of a stand-alone microinverter with push-pull DC/DC power converter.

[27] T.M. Chen, C.L. Chen, Characterization of asymmetrical half bridge fly back converter, in: Proceedings of the IEEE Power Electronics Specialists Conference, 2002, pp. 921–926.

[28] Beibei, R.; Dan, W.; Chengxiong, M.; Jun, Q.; Jiangang, Z. Analysis of full bridge DC-DC converter in power system. In Proceedings of the 2011 4th International Conference on Electric Utility Deregulation and Restructuring and Power Technologies (DRPT), Weihai, China, 6–9 July 2011; pp. 1242–1245

[29] Ikeda, S.; Kurokawa, F. Isolated and wide input ranged boost full bridge DC-DC converter with low loss active snubber. In Proceedings of the 2017 IEEE Energy Conversion Congress and Exposition (ECCE), Cincinnati, OH, USA, 1–5 October 2017; pp. 2213–2218

[30] Famoso, F., Lanzafame, R., Maenza, S., & Scandura, P.F. (2015). Performance Comparison between Micro-inverter and String-inverter Photovoltaic Systems.

[31] Ikkurti HP, Saha S. A comprehensive techno-economic review of microinverters for Building Integrated Photovoltaics (BIPV). Renew Sustain Energy Rev 2015;47:997–1006.

[32] Chiu HJ, Lo YK, Yang CY, Cheng SJ, Huang CM, Chuang CC, et al. A module integrated isolated solar microinverter. IEEE Trans Ind Electron 2013;60:781– 8.

[33] Masia, S. (2009a, April). Integrated module/inverter systems produce rooftop AC. Solar Today Magazine, p. 14.

[34] [Thong Q, Hornic T. Control of power inverters in renewable energy and smart grid integration. Wiley: Chichester, UK; 2013.

[35] S. Refaat, Shady & Abu-Rub, Haitham & Sanfilippo, Antonio & Mohamed, Amira. (2017). Impact of grid-tied large-scale photovoltaic system on dynamic voltage stability of electric power grids. IET Renewable Power Generation. 12. 10.1049/iet-rpg.2017.0219.

[36] Sandia National Laboratories: Stand Alone Photovoltaic Systems: A Handbook of Recommended Design Practices, Springfield: National Technical Information Service, VA, 1988

[37] Solar Electric Supply. (2010). Enphase microinverters. Solar Electric Supply, from https://www.solarelectricsupply.com/solar-components/solar-inverter/enphase

[38] Jabatan Pendidikan Tinggi TV. (2018, December 6). Rise@Uni 2018: Solar kiosk from University of Malaya (UM) [Video]. YouTube. https://youtu.be/DGUaFNIJZLY?si=W2eSrGAd9NPmhCqi

[39] Anuja Namboodiri and Harshal S. Wani, "Unipolar and Bipolar PWM Inverter," *International Journal for Innovative Research in Science & Technology*, vol. 1, no. 7, Dec. 2014.

APPENDICES

APPENDIX A ENPHASE Microinverter Datasheet

IQ8M and IQ8A Microinverters

INPUT DATA (DC)		IQ8M-72-2-US	IQ8A-72-2-US
Commonly used module pairings[1]	W	260 – 460	295 – 500
Module compatibility		54-cell / 108 half-cell, 60-cell / 120 half-cell, 66-cell / 132 half-cell and 72-cell / 144 half-cell	
MPPT voltage range	V	30 – 45	32 – 45
Operating range	V	16 – 58	
Min. / Max. start voltage	V	22 / 58	
Max. input DC voltage	V	60	
Max. continuous input DC current	A	12	
Max. input DC short-circuit current	A	25	
Max. module I_{sc}	A	20	
Overvoltage class DC port		II	
DC port backfeed current	mA	0	
PV array configuration		1 x 1 Ungrounded array; No additional DC side protection required; AC side protection requires max 20A per branch circuit	
OUTPUT DATA (AC)		**IQ8M-72-2-US**	**IQ8A-72-2-US**
Peak output power	VA	330	366
Max. continuous output power	VA	325	349
Nominal (L-L) voltage / range[2]	V	240 / 211 – 264	
Max. continuous output current	A	1.35	1.45
Nominal frequency	Hz	60	
Extended frequency range	Hz	47 – 68	
AC short circuit fault current over 3 cycles	Arms	2	
Max. units per 20 A (L-L) branch circuit[3]		11	
Total harmonic distortion		<5%	
Overvoltage class AC port		III	
AC port backfeed current	mA	30	
Power factor setting		1.0	
Grid-tied power factor (adjustable)		0.85 leading – 0.85 lagging	
Peak efficiency	%	97.8	97.7
CEC weighted efficiency	%	97.5	97
Night-time power consumption	mW	60	
MECHANICAL DATA			
Ambient temperature range		-40°C to +60°C (-40°F to +140°F)	
Relative humidity range		4% to 100% (condensing)	
DC Connector type		MC4	
Dimensions (H x W x D)		212 mm (8.3") x 175 mm (6.9") x 30.2 mm (1.2")	
Weight		1.08 kg (2.38 lbs)	
Cooling		Natural convection – no fans	
Approved for wet locations		Yes	
Pollution degree		PD3	
Enclosure		Class II double-insulated, corrosion resistant polymeric enclosure	
Environ. category / UV exposure rating		NEMA Type 6 / outdoor	
COMPLIANCE			
Certifications		CA Rule 21 (UL 1741-SA), UL 62109-1, IEEE 1547:2018 (UL 1741-SB 3rd Ed.), FCC Part 15 Class B, ICES-0003 Class B, CAN / CSA-C22.2 NO. 107.1-01 This product is UL Listed as PV Rapid Shutdown Equipment and conforms with NEC 2014, NEC 2017, and NEC 2020 section 690.12 and C22.1-2018 Rule 64-218 Rapid Shutdown of PV Systems, for AC and DC conductors, when installed according to manufacturer's instructions.	

(1) Pairing PV modules with wattage above the limit may result in additional clipping losses. See the compatibility calculator at https://link.enphase.com/module-compatibility. (2) Nominal voltage range can be extended beyond nominal if required by the utility. (3) Limits may vary. Refer to local requirements to define the number of microinverters per branch in your area.

IQ8MA-12A-DS-0069-03-EN-US-2022-12-27

APPENDIX B Coding for Perturb and Observe (P&O) Algorithm

P&O

```
function D = PO(Vpv,Ipv)
 Dmax=0.9;
 Dmin=0.1;
 Dinit=0.6;
 deltaD=1e-6;
 persistent Dpre Ppre Vpre;

 %first run
     if isempty(Dpre)
         Dpre=Dinit;
         Vpre=0;
         Ppre=0;
     end
 Ppv=Vpv*Ipv;
 dp=Ppv-Ppre;
 dv=Vpv-Vpre;

     if dp~=0
             if(dp>0)
                     if(dv<0)
                         D=Dpre+deltaD;
                     else
                         D=Dpre-deltaD;
                     end
             else
                     if(dv<0)
                         D=Dpre-deltaD;
                     else
                         D=Dpre+deltaD;
                     end
             end
    else
          D=Dpre;
    end

    if D>=Dmax || D <= Dmin
        D=Dpre;
    end

    Ppre=Ppv;
    Vpre=Vpv;
    Dpre=D;
end
```